DEFORMATION CHARACTERISTICS OF POLYCRYSTALLINE MAGNESIUM OXIDE AT AMBIENT TEMPERATURE

by

A. M. ABDEL-LATIF

A THESIS SUBMITTED TO THE FACULTY OF GRADUATE STUDIES

IN PARTIAL FULFILMENT OF THE REQUIREMENT FOR THE DEGREE

OF MASTER OF SCIENCE OF MECHANICAL ENGINEERING

DEPARTMENT OF MECHANICAL ENGINEERING

University of Manitoba

WINNIPEG, CANADA

December, 1976.

"DEFORMATION CHARACTERISTICS OF POLYCRYSTALLINE MAGNESIUM OXIDE AT AMBIENT TEMPERATURE"

by

A. M. ABDEL-LATIF

A dissertation submitted to the Faculty of Graduate Studies of the University of Manitoba in partial fulfillment of the requirements of the degree of

MASTER OF SCIENCE

CONTENTS

Page

ABSTRACT

The deformation behavior of fully dense, 99.9% pure polycrystalline MgO under uniaxial compression has been investigated. Etch pitting and acoustic emission techniques were employed.

The macroscopic response of MgO under compression, together with the microstructural studies have indicated that MgO exhibits three deformation stages. These are: 1) microplastic, 2) macroplastic, and 3) fracture.

Acoustic emission studies have been used to characterize each deformation stage. The first stage is characterized by a low amplitude signal with low count rate. This signal is assumed to be due to the localized plastic deformation in isolated regions of the grains. The second stage is characterized by two signals; a low amplitude signal similar to that observed in stage (1) and a high amplitude signal which we assume is resulting from the microcrack initiation. The third stage is characterized by the emission of three different signals: (1) and (2) similar to those observed in stages 1 and 2. The third signal is a medium amplitude which is proposed to accompany crack propagation.

The effect of grain size on the fracture stress has been investigated. A non-linear behavior between σ_f and $D^{-1/2}$ is observed. A correlation between the cumulative number of AE events and strain was found to follow an equation of the form

$$\Sigma\phi = Q \cdot \varepsilon^{A}.$$

ACKNOWLEDGEMENTS

I wish to acknowledge the help of my supervisor Professor K. Tangri during the course of this work. Thanks are due to my friend Dr. N. Ibrahim for his suggestions and discussions and to Professor N. Popplewell for reading the original manuscript.

The financial support provided to me through grants from AECL and a graduate fellowship from The University of Manitoba is greatly appreciated.

Special gratitude is due to my wife for her encouragement and sacrifices during the course of this study.

LIST OF TABLES

LIST OF FIGURES

Page

CHAPTER I

INTRODUCTION

Acoustic emission may be defined as the stress waves generated during the dynamic processes in materials. Acoustic emission technique is very sensitive to local instabilities such as: the formation of a slip band, initiation of a microcrack and propagation of cracks. Thus, AE technique records events while they are taking place and can be used to identify different AE signals characterizing different deformation mechanisms.

Considerable amount of data are now available in the literature on the macroscopic response of polycrystalline MgO under various loading conditions. However, a correlation between microstructural aspects of deformation and macroscopic response of the material is lacking. Also, previous studies on AE of MgO were limited to bending tests on precracked specimens. Thus, a detailed study on the deformation behavior of MgO under uniaxial loading is needed in order to delineate the role of microstructure.

This thesis is concerned with the deformation characteristics of polycrystalline MgO in compression at ambient temperature. AE techniques together with etch pitting studies were used in order to correlate macroscopic response with the microstructural features developing during deformation.

The objectives of this study are as follows: firstly, to monitor and characterize the AE signals associated with different loading levels during compression and to relate these signals to possible energy dissipating processes, and secondly, to study the effect of grain size on the macroscopic response of the material.

CHAPTER II

LITERATURE REVIEW

This review is organized as follows: section 1 reviews the history, basic concepts and parameters of acoustic emission (AE) and work done on ceramics. Section II considers the effect of the microstructure on the mechanical properties of polycrystalline MgO and the relation of the microstructure variables to AE.

2.1.1 Acoustic emission, history and definition

Acoustic emission is the term used to describe the phenomenon of the generation of acoustic signals in stressed materials. When a specimen is loaded, the potential elastic energy is stored in the specimen. This stored energy increases until the state of plastic deformation is reached. At this moment part of the stored elastic energy is transformed into acoustic emission. Many local instabilities are considered sources of acoustic emission (AE). Pollock [1] reviewed the origin of acoustic emissions; and related it to the microscopic strain fields surrounding a dislocation, or the microscopic strain field which drives a crack forward in a stressed structure. Liptai [2] et al reported that emission activity was related to pile ups and breakaway of dislocations. Twinning, martensitic phase transformations, and the interaction of dislocations with surfaces are also possible sources of acoustic emission.

Bill [3], Dunegan and Tatro [4] and Bellosillo [5] reviewed the history of acoustic emission. It was reported that the work of Kaiser was the origin of modern work in acoustic emission. Kaiser [4] discussed the low intensity sound waves given off by a material due to deformation

in tension. He reported that these sounds are irreversible and therefore the mechanisms which give rise to them are also irreversible. Schofield [6] reported that acoustic emission from metals was the result of dislocation motion during plastic deformation. The results of his experiments on Al single crystals showed that a greater number of acoustic emissions was observed in single crystals which underwent multislip rather than those which underwent slip on one slip system. He reported a correlation between the number of acoustic emissions and the strain [7]. Another interesting observation was that there is a relation between the slip lines appearing on the surface of the crystal and acoustic emission during deformation.

An important conclusion was that AE is a volume and not a surface effect. This conclusion is similar to the observations reported by Dunegan and Tatro [4].

Dunegan et al [8] investigated the AE behaviour from Beryllium. They reported that AE resulting from flawed specimens began at stress levels far below the general yield stress. They found that the total number of AE should be proportional to the fourth power of the stress intensity factor obtained from crack fracture mechanics. Liptai et al [2] showed that AE from an initially flaw-free metal specimen, consists of two components:

1. Low level continuous emission which appears in the early loading stages.
2. High level burst - This component does not occur continuously. - It is usually of higher amplitude than the first component, and is associated with microcrack formation.

Dunegan et al [9] plotted the stress and the rate of acoustic emission as a function of strain, for a Beryllium tensile specimen. They observed a large increase in the rate of AE just before the yield stress. This result is similar to the behaviour of 7075-T5 Al. They reported that as the strain was increased beyond the yield point, the rate of emission declined [10]. It was also reported that more AE is observed from high strength brittle materials, which is consistent with the higher energy levels associated with the dislocation processes in these materials.

2.1.2 Acoustic emission and deformation

Fisher and Lally[11] proposed that an acoustic emission burst will be produced if the applied stress is of sufficient value to activate dislocation sources so that dislocations can spread across the specimen. However, calculations showed that the dislocations should have a very high velocity at the applied stress on the specimen. They suggested that the stress concentrations which develop at the head of the slip bands are capable of activating other dislocation sources and produce AE.

The application of AE techniques to monitor the deformation in rocks and ceramics has received growing attention. Thill [12] monitored the AE events during the deformation of rocks in compression. The AE technique was used to determine the deformation characteristics in the rock under stress. AE pulse velocity, amplitude and total events were correlated with stress-strain data. Through the velocity data, Thill defined the level of stresses and deformation regions on the basis of Bieniawski's Mechanism [13]. The deformation stages[12] which were

recognized were: crack closure - linear elasticity - fracture initiation and development - accelerated fracture and gross fracture. Several observations were made: firstly, the number of AE count[5] and the count rate increase as the applied stress approached the fracture stress [18], secondly, at higher stresses the amplitude of the pulses is nearly constant and undergoes little or no increase with further increase in stress.

Noone and Mehan [15] described the detection and observation of discrete events taking place during the deformation of ceramics in bending. They tried to correlate the AE during the test with visual observations on the microstructure of specimens during the test. Cracks were introduced into the specimens by subjecting them to thermal shocks. They observed that AE is apparently related to the volume of the specimen under stress, and that as the grain size was increased the acoustic emission activity increased. Their conclusion was that AE was a result of intergranular cracking. Graham and Alers [16] investigated the conditions under which AE signals are generated in ceramics prior to fracture. They performed their tests on polycrystalline MgO, Al_2O_3 and MgO single crystal. A correlation was proposed between the cumulative number of AE bursts and the area swept out during the motion of a slowly advancing crack front. It was observed that in lucalox the size of the area associated with one acoustic emission burst was nearly equal to the area of one grain. As for Magnesia the area per burst correlated best with the size of a grain boundary facet instead of the entire grain. It was observed that the frequency spectra obtained for individual AE signals generated during the plastic deformation of MgO single crystals was similar to the spectra observed in a variety of materials.

Gillis and Hamstad [17] investigated the relationship between AE and deformation in terms of the dislocation mechanisms which are likely to produce AE. They proposed a mathematical theory to estimate the relation between the observed number of AE counts and plastic strain. The conclusion was that AE may be associated only with a small fraction of the total plastic strain, therefore it is difficult to correlate AE with the total strain.

Recently, Evans and Graham [18] developed a mathematical model for macrocrack propagation in polycrystalline ceramics. This model is based on the experimental acoustic emission amplitude studies. The basic idea of their model is that the crack front is contoured in accord with the microstructural features such that the crack moves forward intermittently at sequential locations along the crack front. Their conclusion was that the crack moves forward in discrete variable amplitude events.

Tandon and Tangri [19] used AE technique to study the dislocation processes occurring at different strain levels during the deformation of Fe - 3% Si. They explained the occurence of AE signals in the microyielding and macroyielding regions to be due to dislocation generation from grain boundary sources. They noticed that the total acoustic emission counts in the microyielding region increased with increasing grain size. This was interpreted as an increase in the density of activable grain boundary sources due to the expected increase in ledge dimensions in a coarse grained material.

2.2 Effect of microstructure

This section considers the influence of microstructure on the deformation behavior of polycrystalline ceramics that have rock salt

structure. MgO is a good example of the ceramics of this category in which fracture can be studied from the dislocation mechanics point of view. In the first part the mechanisms of fracture will be reviewed, the second part considers the effect of grain size on the plastic deformation and its relation with the acoustic emission parameters, such as count rate, total emission events and amplitude.

2.2.1 Mechanisms of fracture

MgO has NaCl structure, but at room temperature, the slip is restricted to the {110} <110> family of slip systems. Due to the failure of {110} <110> slip to provide five independent slip systems required by the von Mises-Taylor criteria for ductiligy, MgO shows very limited plasticity before fracture. In this case the plastic strain is accompanied by a large amount of stored elastic energy, thus enhancing cleavage fracture [20]. Many theoretical models have been developed to describe the fracture behavior of rock salt type ceramics. Originaly Zener [21] suggested that the concentrated stresses that develop at the head of a pile up of dislocations may cause the leading dislocation to coalesce and thus form a crack nucleous. This concept was developed further by Petch [22] who concluded that two mechanisms are likely to nucleate cracks. The first mechanism is the nucleation of a crack by slip band. The basic idea is that when dislocations pile up against a grain boundary, the stress concentration at the head of a slip band is sufficient to initiate a crack. The second mechanism is the nucleation of a crack by the intersection of slip bands. When broad slip bands meet, they are unable to penetrate fully and a stress field is set up. This stress field at the intersection is relieved by cracking.

Averback [23] reviewed the physical aspects of fracture and proposed that the formation of microcracks is a result of localized plastic deformation. This localized plastic deformation supplies the stress concentration necessary for both the initiation and propagation of a crack. The net plastic deformation over the entire specimen may be small but is is localized in the grains along which the crack travels.

Cracks have been observed to form at slip band intersections in polycrystalline MgO [24]. In this case if two conjugate slip bands intersect, a stress concentration will be created at the point of intersection. Kear et al [25] reviewed the possible dislocation reactions in ionic crystals with NaCl structure. Three possible dislocation reactions are likely to take place in MgO at ambient temperature.

$$a/2\ [0\bar{1}1] + a/2\ [\bar{0}11] \rightarrow a\ [001] \qquad (1)$$

$$a/2\ [\bar{1}01] + a/2\ [\bar{0}11] \rightarrow a/2\ [\bar{1}10] \qquad (2)$$

$$a/2\ [10\bar{1}] + a/2\ [0\bar{1}\bar{1}] \rightarrow a/2\ [1\bar{1}\bar{2}] \qquad (3)$$

The first reaction will not take place as the elastic energy is not reduced. However the dissociation of a $[00\bar{1}]$ dislocation into a pair of a/2 $[00\bar{1}]$ will result in the creation of a stacking fault of high energy. Only reaction (2) occurs since it leads to a reduction in the elastic energy. The third reaction is unlikely since it involves an increase in energy.

The steps leading to dislocation initiated fracture in a crystalline solid were suggested by Conrad and Sujada [26]. These steps are shown in figure (1).

Bieniawski [13] reviewed the basic concepts and theory of fracture. Based on his data, he postulated a mechanism for the brittle fracture of rock in compression. A schematic representation of this mechanism is shown in fig. (2). Marsh [27] investigated the stress concentration at the steps on crystal surfaces and their role in fracture. He concluded that steps present stress concentrations comparable in magnitude and nature to those of cracks of similar dimensions.

2.2.2 Effect of Grain Size

Grain size has a significant effect on the microplastic behavior of a specimen. Low [28] pointed out that variation in grain size is expected to influence brittle fracture in the following way: the grain size effect is caused by the change in the stress concentration with the change in the length of the slip band. As the grain size increases the uninterupted slip distance increases therefore, the probability of crack nucleation is expected to increase [29].

Averbach [23], in his review of the physical aspects of fracture, related grain size to the length of the slip band as follows:

$$\sigma_f = q_c(\sigma_y - \sigma_o) \tag{4}$$

$$P_c = q_c \cdot b \tag{5}$$

$$q_c = C \cdot d^{1/2} \tag{6}$$

$$P_c = f \cdot d^{1/2} \tag{7}$$

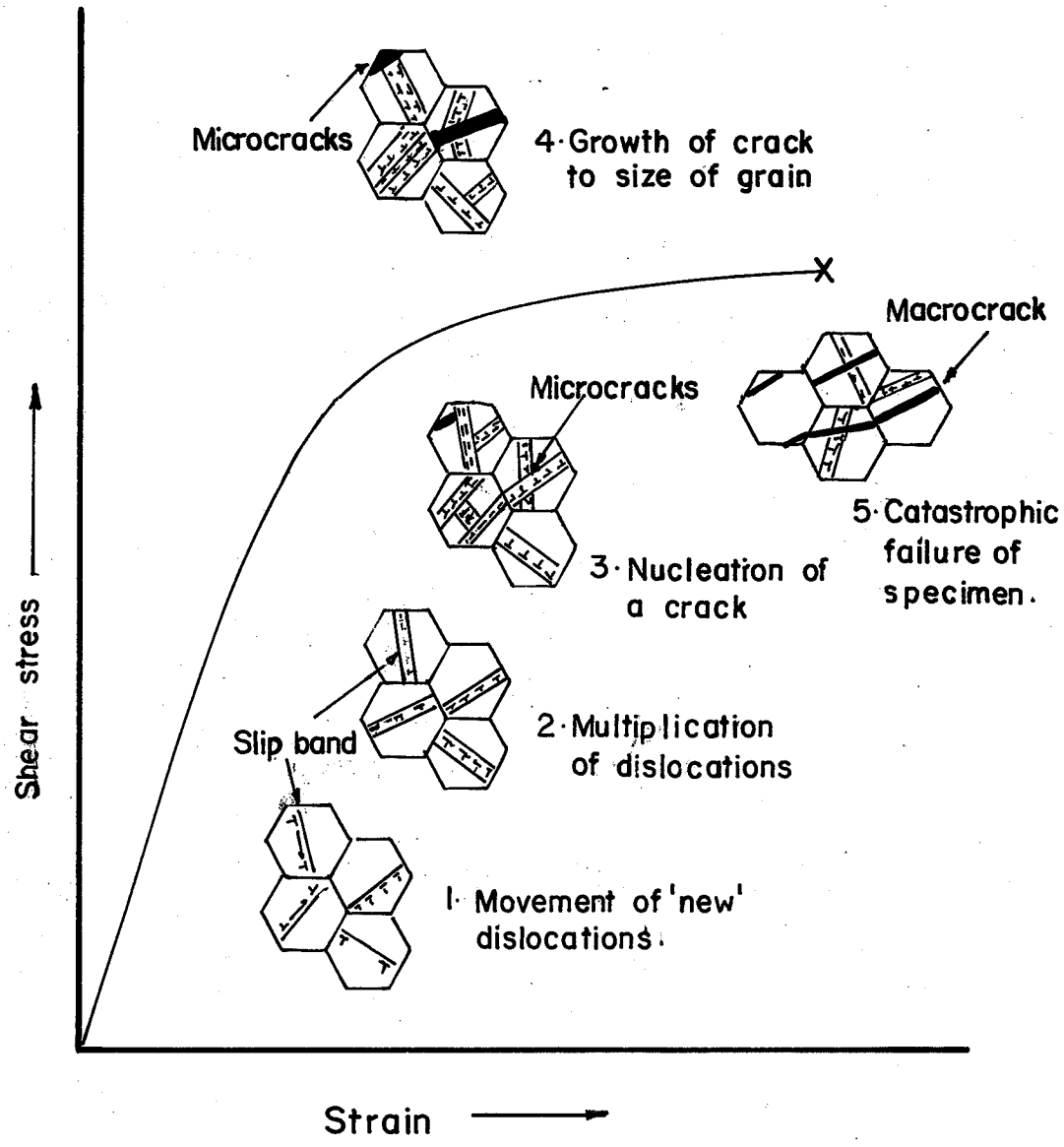

Fig.(1) Schematic of the steps leading to fracture of a semibrittle solid in tension. (After H·Conrad and E Stofel)[30]

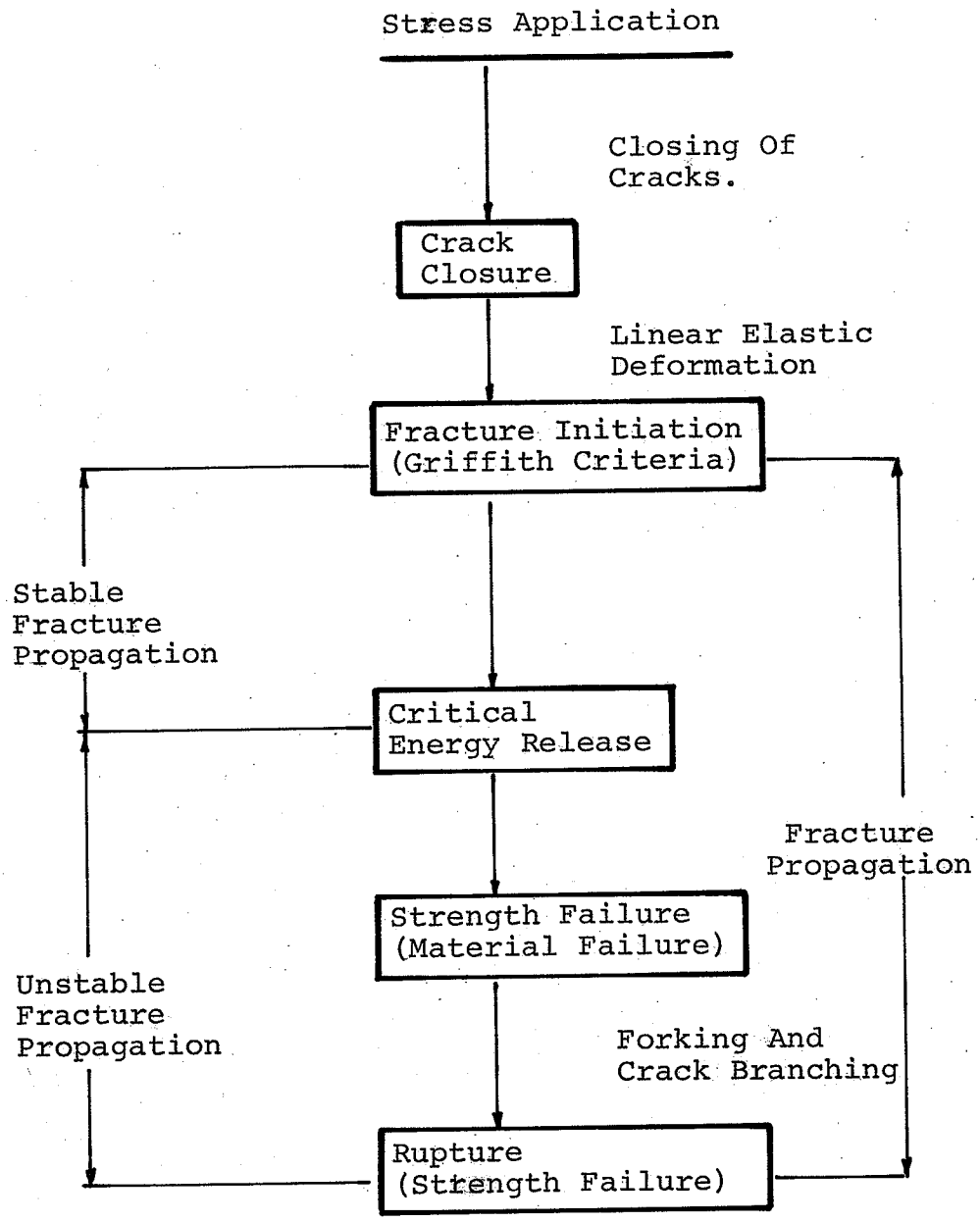

Fig.(2) Bieniawski's scheme for considering rock fracture in compression. (After R.G.Liptai et. al.)[2]

where

σ_f is the fracture stress, σ_y is the yield stress, σ_o is the friction stress, q_c is the stress concentration at the head of the slip band, P_c is the width of the slip band, d is the grain diameter, b is the Burger's vector, C and f are constants. The conclusion is that: a thicker slip band is required to initiate fracture as the grain size increases.

Davidge [30] investigated the influence of grain size on the fracture strength of fully dense polycrystalline MgO. The Hall-Petch equation [31] was proved to be valid. Carniglia [32] re examined equations relating the tensile strength of polycrystalline ceramics to the grain size. His examination of 30 sets of data led him to conclude that Orwan and Petch's equations fit these data.

Sinha et al [33] investigated the plastic flow in polycrystalline MgO prior to fracture at ambient temperature. It was shown that the initial generation of dislocations occurs at a stress independent of the grain size and below the microyield stress. It was concluded that both the fracture and yield stresses follow Hall-Petch relationship. Tandon and Tangri [19] investigated the acoustic emission from polycrystalline Fe - 3% Si. They noticed that as the grain size increases the total number of acoustic emissions tend to increase in the microyield region. They interpreted their results in terms of grain boundary ledges and activation of grain boundary dislocation sources. Noone and Mehan [15] investigated the crack propagation in ceramic materials in bending. They observed that as grain size was increased, acoustic emission activity increased. This was explained to be due to the integranular cracking in coarse grain ceramics.

CHAPTER III

EXPERIMENTAL PROCEDURE

3.1 Preparation of specimens

All the experiments were performed on fully dense, 99.9% pure MgO which was obtained from Eastman Kodak Company, U.S.A. The specimens were bars 16 mm long and of a square cross-section of 6 x 6 mm. The geometry of the specimen provided an optimum length to width ratio (L/W). Since, if (L/W) is more than 3, the failure would be due to the buckling and if (L/W) is less than 2.5 the friction stress between the specimen ends and grips would affect the results [34].

In order to minimize surface defects such as microcracks, special care was maintained throughout handling and mechanical polishing. The surfaces of the specimens were mechanically polished using diamond paste followed by chemical polishing in a hot solution of 85% orthophosphoric acid. Chemical polishing was repeated after heat treatment. The specimens were then divided into batches and a range of grain sizes of 20 to 400 micron was produced by heating at 1650 C for various periods of time. The specimens were left to cool in the furnace.

3.1.1 Grain size measurements

The line intercept method was used in the measurement of grain size. (Details of the method are given in Appendix 1). The average grain diameter (D) was calculated using the equation:

$$D = L/N \times M$$

where: L = total length of traverse lines

M = magnification

N = total number of grains intercepting the traverse lines.

3.1.2 Etch pitting studies

Etch pitting investigations were performed to determine the initial dislocation density (ρ_o) in all the specimens. The etching was performed in a solution of 50% H_2SO_4 plus 50% H_2O at 53 °C. Twenty five representative grains in different areas were selected and the number of dislocation etch pits was counted. The initial dislocation density was calculated using the following equation:

$$\rho_o = \frac{\text{total number of etch pits}}{\text{area of the grains}}$$

Assuming that the grains are circular, then:

$$\rho_o = \frac{4 \times Q}{25 \pi D^2} = 5.09 \times 10^{-2} \frac{Q}{D^2}$$

where Q is the number of dislocation etch pits.

3.2 Description of AE equipments and set up

Acoustic emission monitoring was conducted using a detection and recording system developed in the Metallurgical Science Laboratory for AE studies. The block diagram of both the monitoring and data analysis systems are shown in figures (3) and (4) respectively. A wide band (.1 - 1 MHz) Dunegan S 9201 transducer was employed in this investigation.

The output signals from the transducer were amplified and recorded on a multichannel magnetic tape. The set up permits the display of data on an X - Y recorder and on an oscilloscope screen. Figure 5 shows the layout of AE system used in this work.

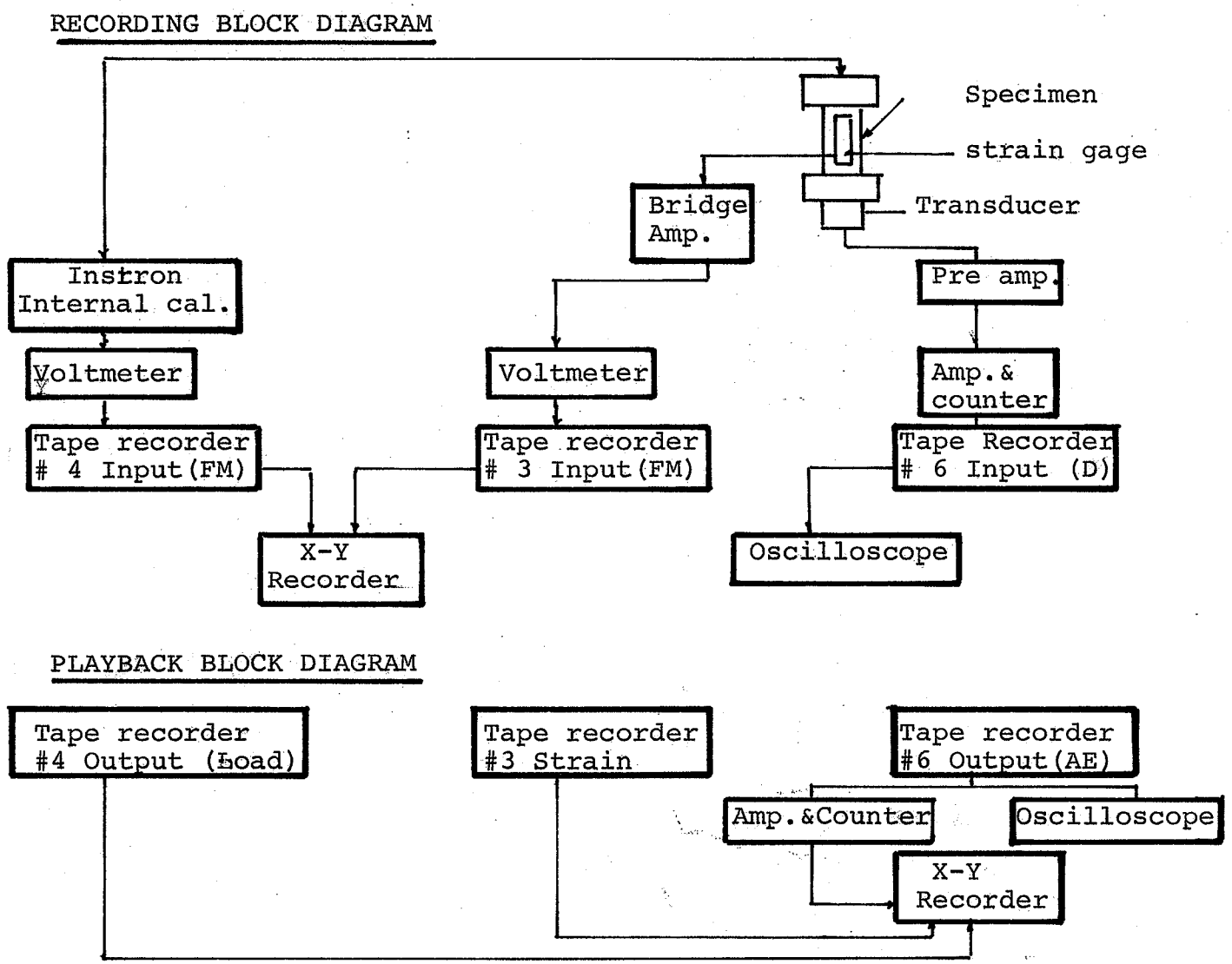

Fig.(3) Schematic diagram of the instrumentation used in the monitoring and recording of acoustic emission during the testing of polycrystalline MgO in compression.

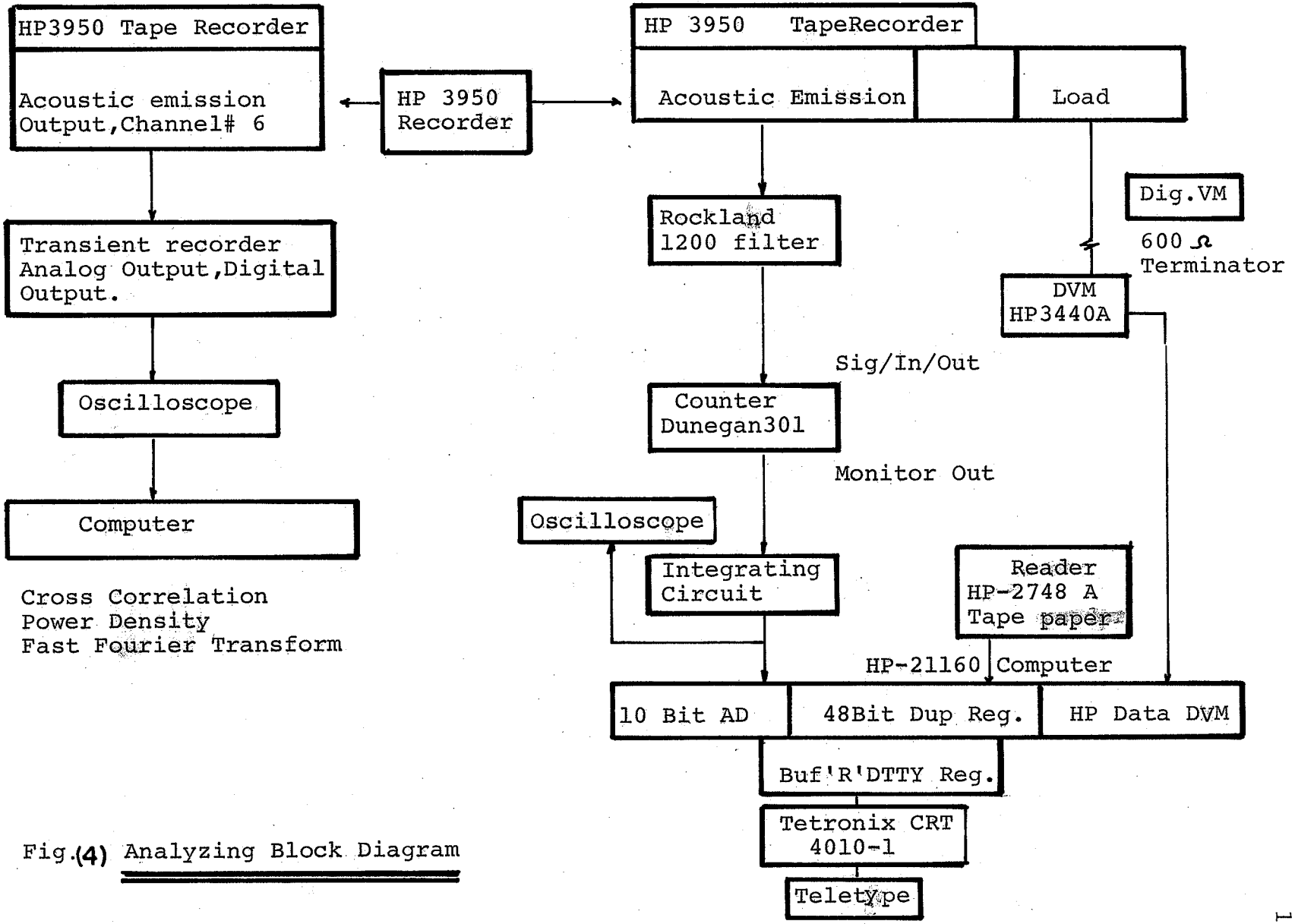

Fig.(4) Analyzing Block Diagram

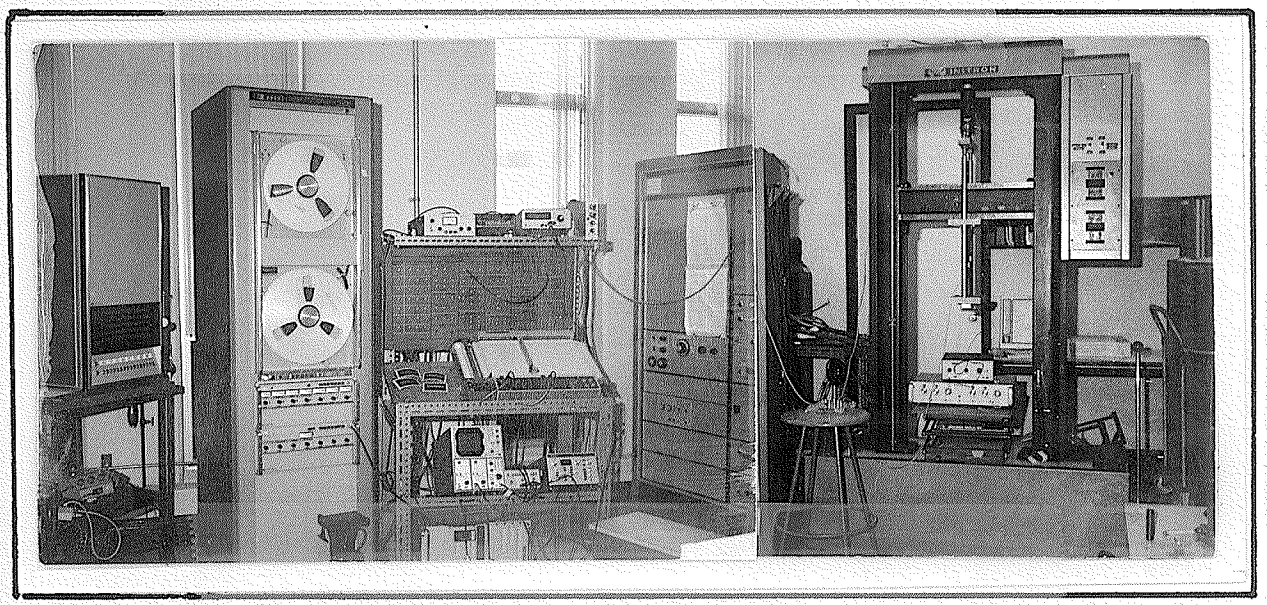

Fig.(5) Arrangement of acoustic emission set up and testing machine.

3.3 Test procedure

All the data to be reported here was obtained in compression at ambient temperature. The compression tests were conducted in an Instron machine, using a cross-head speed of 0.01 cm/min, which yielded a strain rate of 10^{-4} $second^{-1}$ in the specimen. The strain was measured using a precalibrated precision strain gage glued to the surface of the specimen using M bond 200 adhesive supplied by M line accessories of Michigan, U.S.A. A layer of grease was applied on the upper and lower ends of the specimen and the jig to prevent noise due to the seating of the specimen during the test.

The transducer was affixed at the bottom of the lower grip as shown in figure (6). To provide acoustic coupling a layer of vacuum grease was applied on the face of the transducer which was clipped tightly to the bottom grip.

Total amplification of the transducer signal was adjusted to a level at which the background (ambient and equipment noise) would not trigger the preset 1 volt threshold of the counter. Unless specifically states, a total gain of 76 dB (which gave an effective trigger level of 158 u volts for the signal) was employed in all the acoustic emission tests. During the tests AE signals were monitored using an oscilloscope. The output of the transducer, after amplification was recorded on a direct channel of a multichannel magnetic tape recorder. The tape speed was 60 inch/second which allowed frequencies up to 350 Khz to be recorded. The DC signals from the load cell and the strain gauge were recorded simultaneously on FM channels.

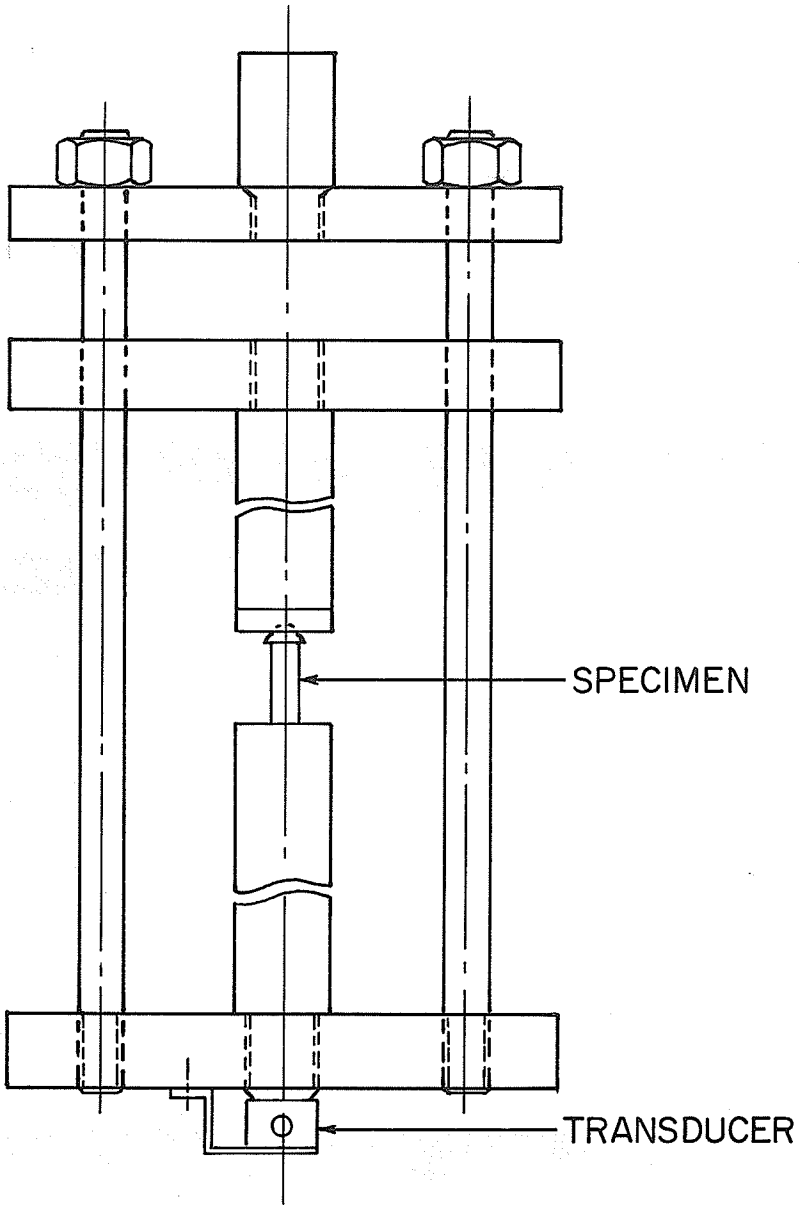

Fig. (6) Detailed diagram of the jig used in the compression tests showing the location of the specimen and the detecting transducer.

To analyze the AE data on the tape a computer program has been developed to yield a final output data in the form of teletyped or displayed graphical data of the following parameters: Load, count rate , total counts, average amplitude of the events, peak amplitude, total energy of emission and the average energy/event. For further analysis of the acoustic emission signals, the stored AE data on the tape were run through a transient recorder which permitted the storage and display of AE data with the aid of an oscilloscope. The different wave forms of AE signals in different regimes of the stress-strain curve were displayed on the oscilloscope screen and photographed.

Full analysis of the AE, load and strain data was conducted on specimens of different grain sizes. Some specimens were saved after being loaded up to 99% of the fracture stress where an observable increase of the acoustic emission activity was detected. These specimens were unloaded and examined by an optical microscope to determine the changes in the microstructure of the specimens. Etch pitting studies were conducted on those specimens using an etchant of 50% H_2SO_4 in water.

3.4 Limitations of the technique

The following limitations are likely to effect the experimental data:

1. The attenuation of acoustic emission signals, from all possible sources other than the specimen during their travel through the grips and cables before recording: this attenuation was assumed to be the same during all the tests as the same set up was used in all the tests.

2. Acoustic emission signals of amplitudes lower than the trigger level of the system are not recorded or detected. The number of AE counts measured with a counter is given by the number of times the amplified sensor signal exceeds the preset threshold voltage of the counter. As such, a single event within the test piece does not produce a single count but may result in several counts, then the actual number of counts depends upon the amplitude of the signal.
3. Other sources are likely to produce AE:
    1. The deformation of the compression jig: this possibility was minimized by using the jig to compress a dummy specimen to a stress higher than the fracture stress of the smallest grain size of MgO specimen. This was done, because acoustic emissions are known to be irreversible.
    2. The friction due to the movement of cross head of the Instron machine with respect to the jig rods: to overcome such a possibility a ring of tephelon was inserted around the rods to reduce AE resulting due to friction.

CHAPTER IV

EXPERIMENTAL RESULTS

All the data reported here were obtained in compression. The results are presented in the following order: (1) Macroscopic response, (2) Microstructural observations and (3) Acoustic emission data collected during the deformation.

4.1 Macroscopic response

Figure (7) shows a typical stress-strain curve of polycrystalline MgO under compression. Three deformation stages (I, II and III) have been defined as: microplastic, macroplastic and fracture respectively. The region corresponding to each stage is marked on the curve of figure (7). It is apparent that, the material exhibits linear behavior up to the microyield stress and this behavior is followed by a non linear behavior up to fracture. Figure (8) demonstrates the relationship between grain size and the total strain ε_f. It shows that as the grain size increases the total strain decreases. This is consistent with the data in uniaxial tension reported in earlier works [39] and [43]. Figure (9) shows the fracture stress-grain size relationship. It can be seen that as the grain size increases the fracture stress decreases. Figure (10) is a plot of the fracture stress versus $1/\sqrt{D}$. It appears from the figure that the Hall-Petch relationship is not strictly obeyed in compression. The shape of the curve suggests a non linear relationship between the fracture stress and $1/\sqrt{D}$.

4.2 Microstructural Observations

The results of the measurement of the initial dislocation density (ρ_o) in all samples of various grain sizes are shown in table (I)

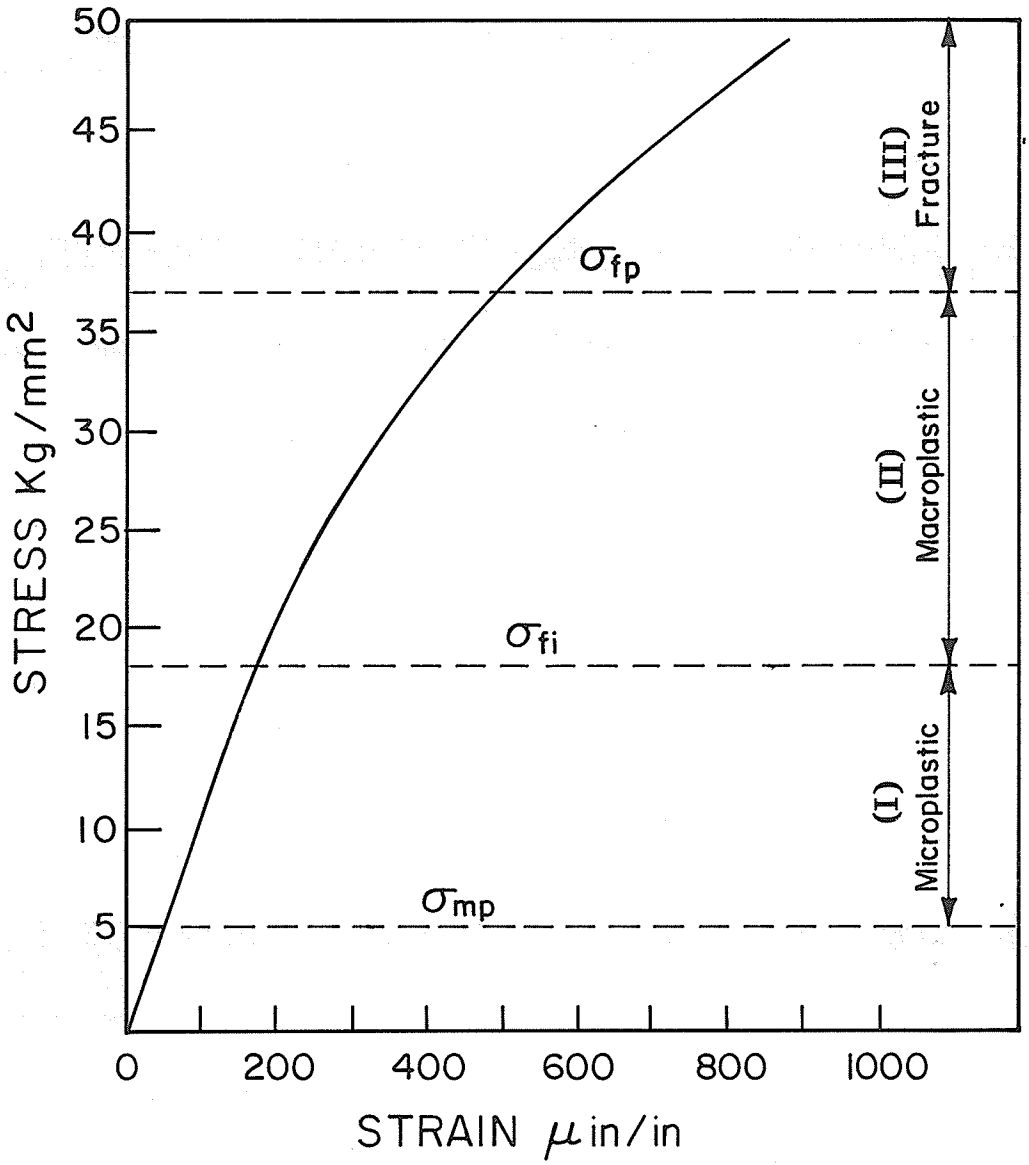

Fig. (7) Stress - Strain diagram of 30 μ Grain size polycrystalline MgO under compression at ambient temperature. Strain rate $\doteq 2 \times 10^{-5}$ second^{-1}

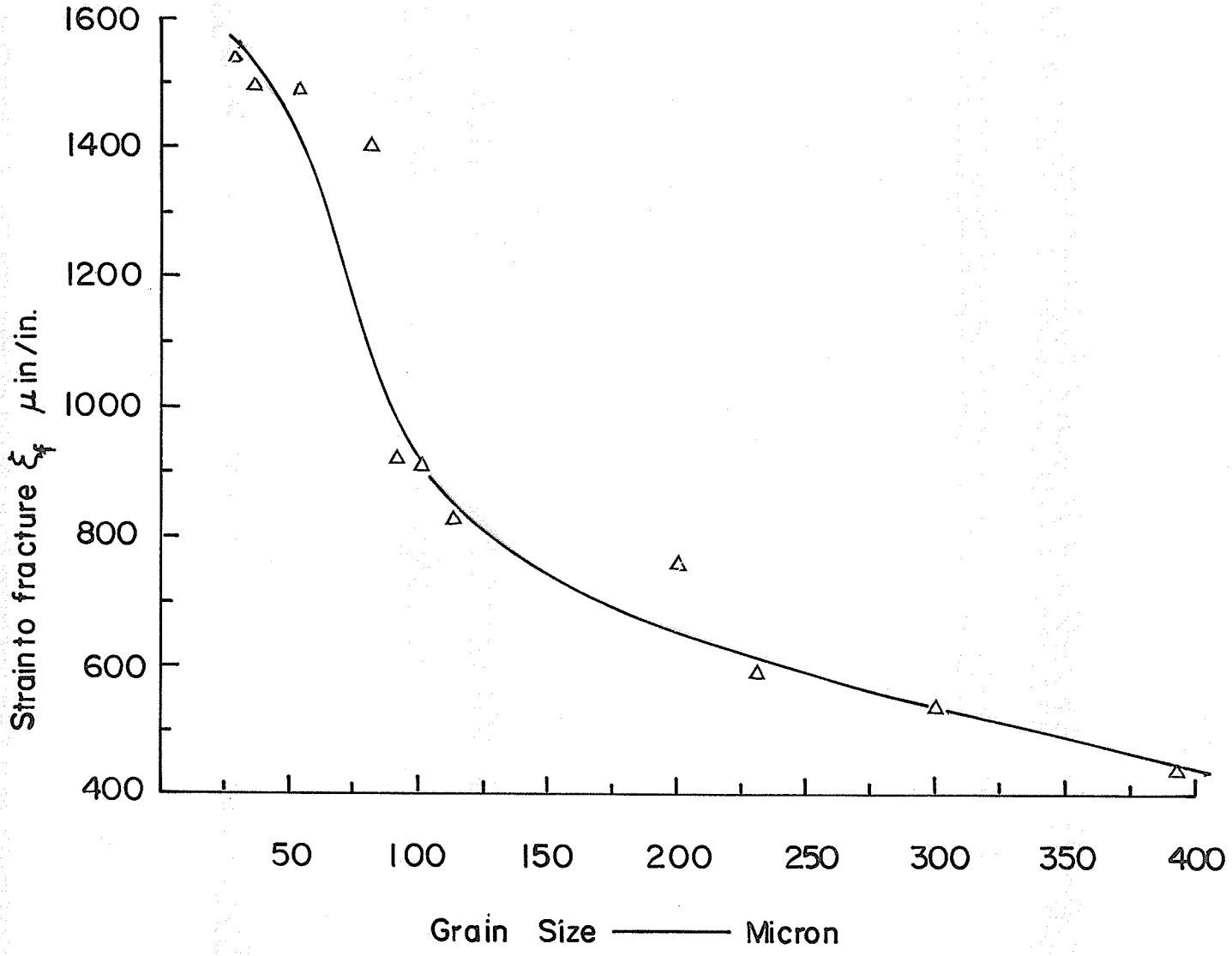

Fig (8) Strain to fracture ξ_f in compression vs. grain size for polycrystalline MgO. Strain rate = 10^{-4} second^{-1}.

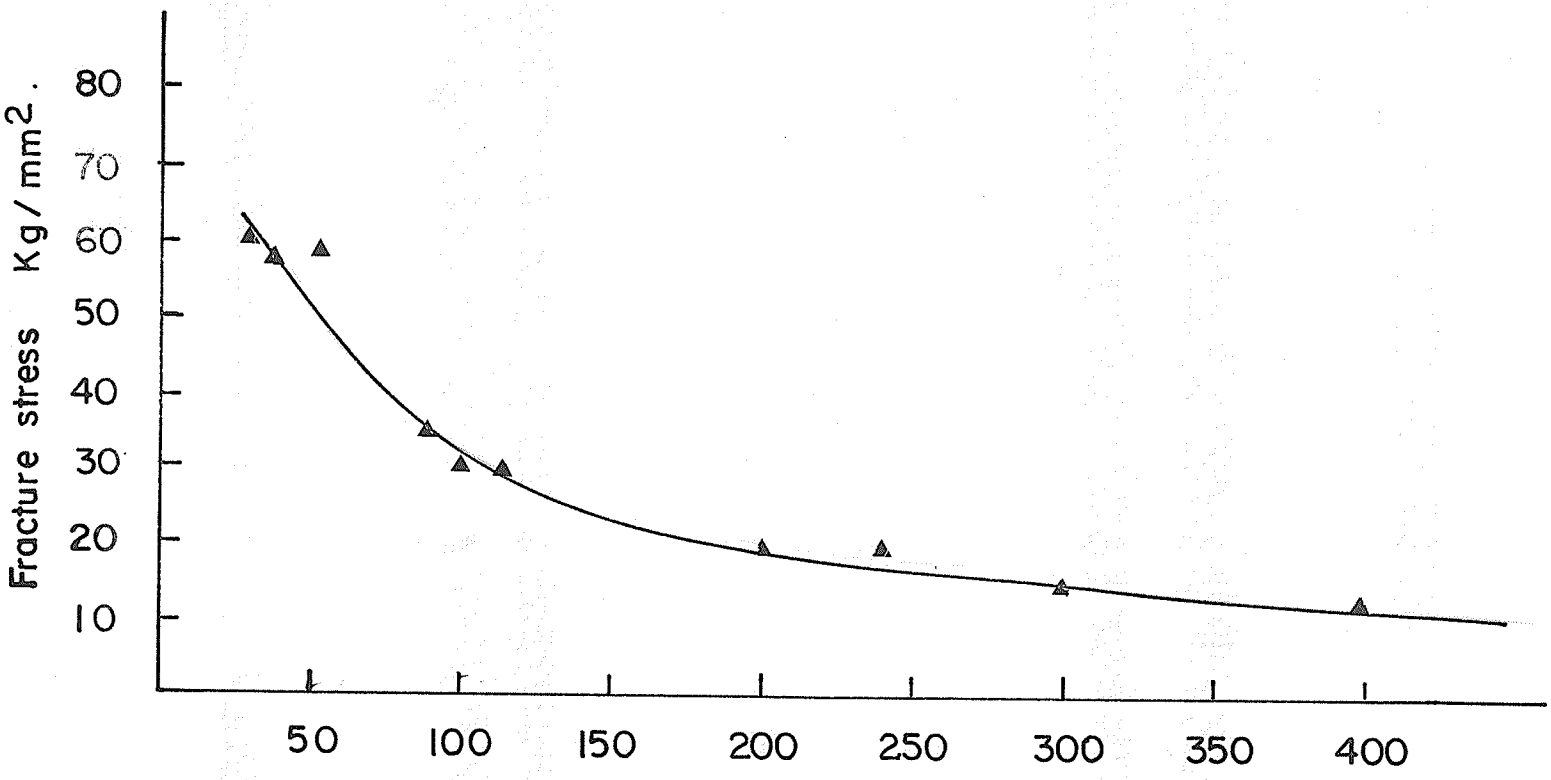

Fig. (9) Fracture stress vs. grain size for polycrystalline MgO.
Strain rate = 10^{-4} second^{-1}.

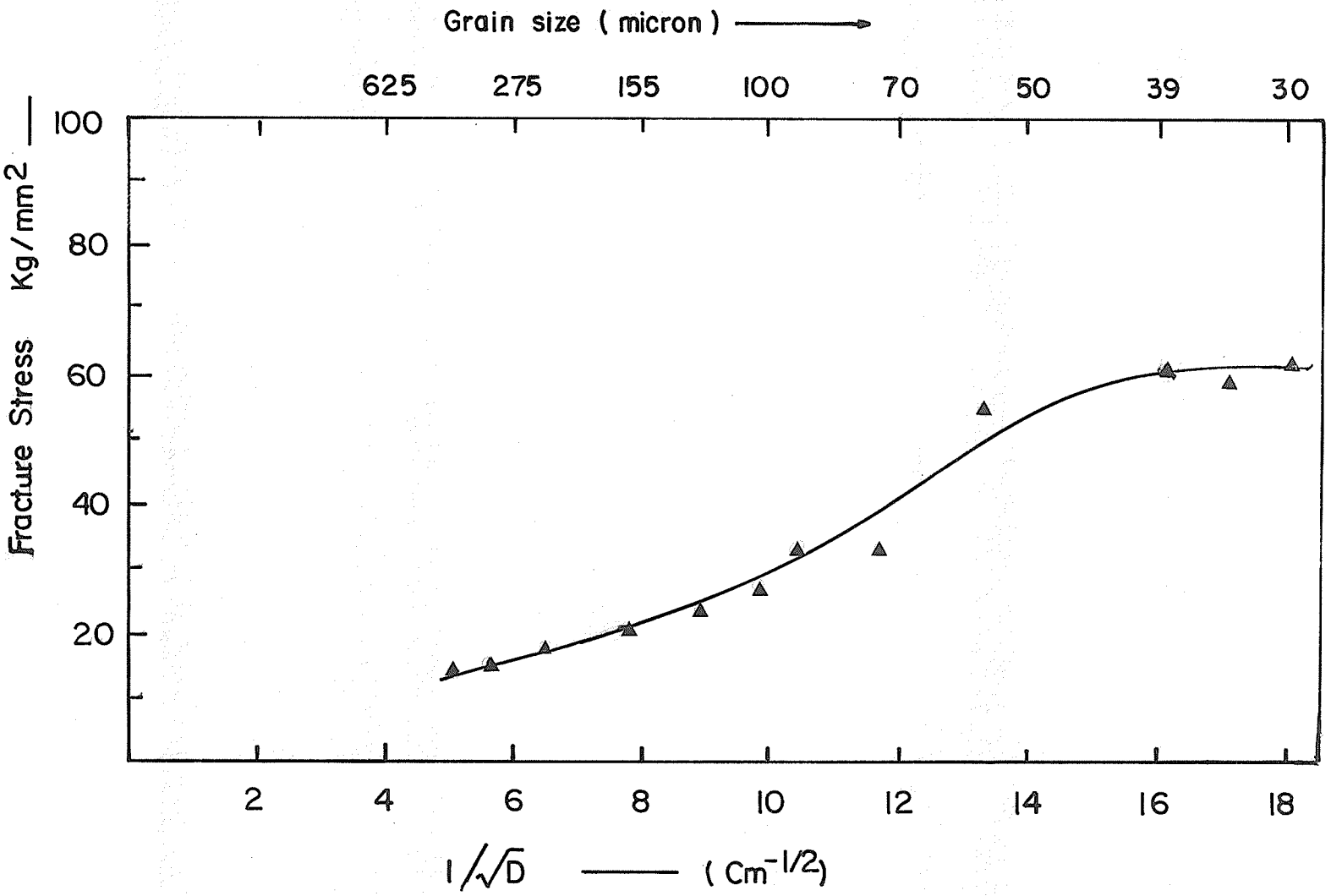

Fig.(10) Fracture stress vs. $1/\sqrt{D}$ for polycrystalline MgO in compression. Strain rate = $1{\cdot}0 \times 10^{-4}$ second^{-1}

and figure (11). The data suggests that, as the grain size increases the initial dislocation density decreases.

Figure (12) shows a typical micrograph of annealed MgO specimen. It can be seen that the specimen is free from cracks and surface damage. Figure (13) shows the slip initiation in some grains at the microyield stress levels. Figure (14) shows the slip activity in the grains at the end of stage I as indicated on figure (7). Figure (15) shows the initiation of microcracks due to the obstruction of slip bands at the grain boundary. In this case, the grain boundary acts as a strong barrier due to the unfavorable orientation of grain A. Thus, the relaxation of high stress concentrations at the tips of slip bands results in the formation of microcracks. Figure (16) shows that the crack propagates transgranularly. Figure (17) shows a typical micrograph for an area surrounding a propagating crack. It should be noted that, the crack is accompanied by an extensive dislocation activity.

Figure (18) is a typical composite micrograph for a polycrystalline MgO specimen just before fracture. Some interesting features may be seen; firstly the cracking has taken place in the specimen with the main crack travelling parallel to the loading direction and secondly, there are some secondary cracks in the grains surrounding the crack front.

The following figures show the microstructural features illustrating the various energy dissipating processes. Figure (19), shows that MgO exhibits plastic deformation in some grains as it was

Table I

Initial dislocation density as determined by etch pitting of polycrystalline MgO samples with different grain sizes.

Average Grain diameter (D) microns	Initial Dislocation Density (ρ_o) x 10^{-5} disl./cm^2	Number of Samples
18	25.60	1
25	15.34	6
31	19.80	7
38	12.52	2
45	7.59	2
55	9.98	3
77	3.10	2
95	1.77	4
120	1.11	2
220	0.26	3
395	0.20	1

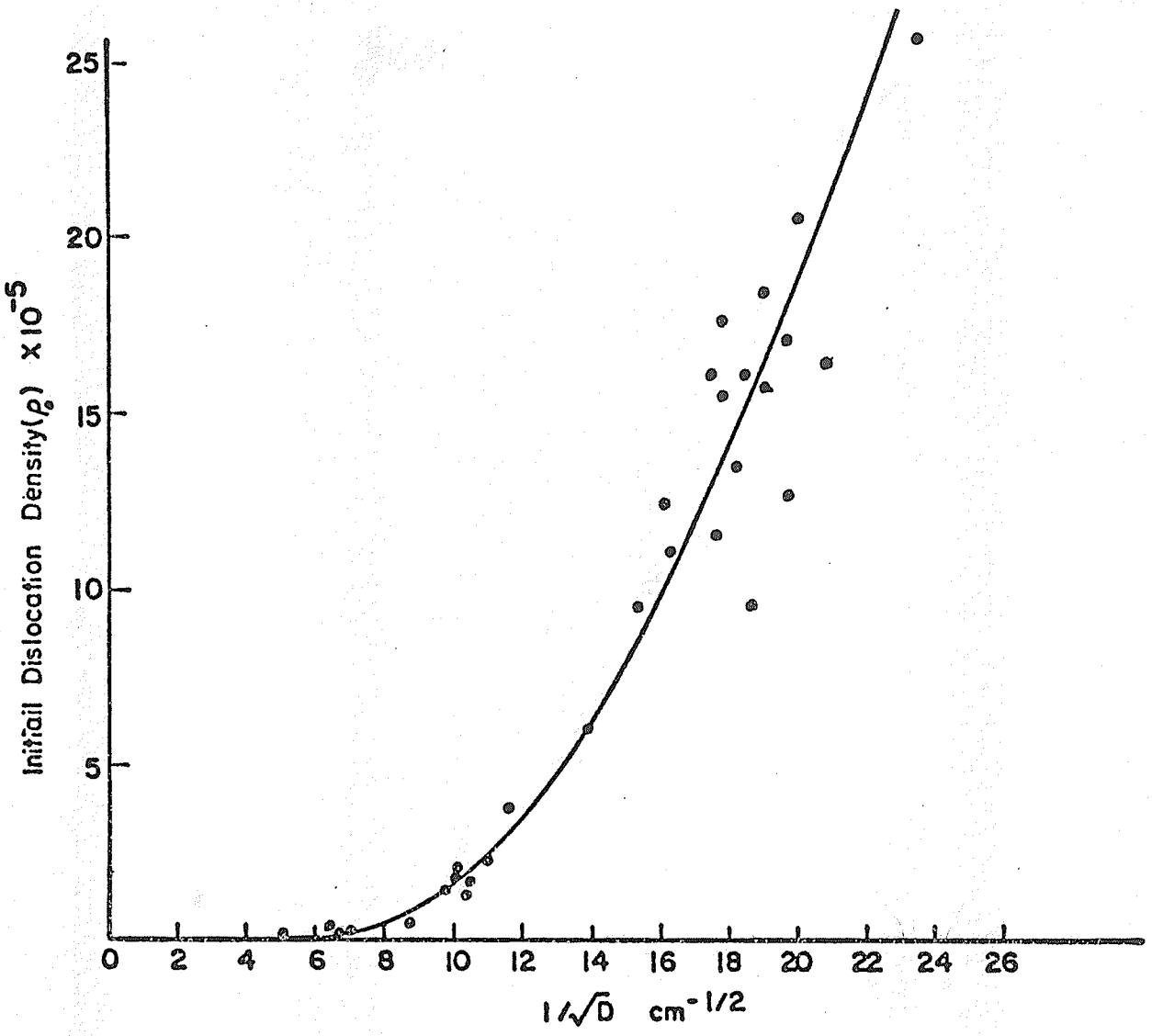

Fig. (11) Initial dislocation density(ρ) as measured in annealed samples.

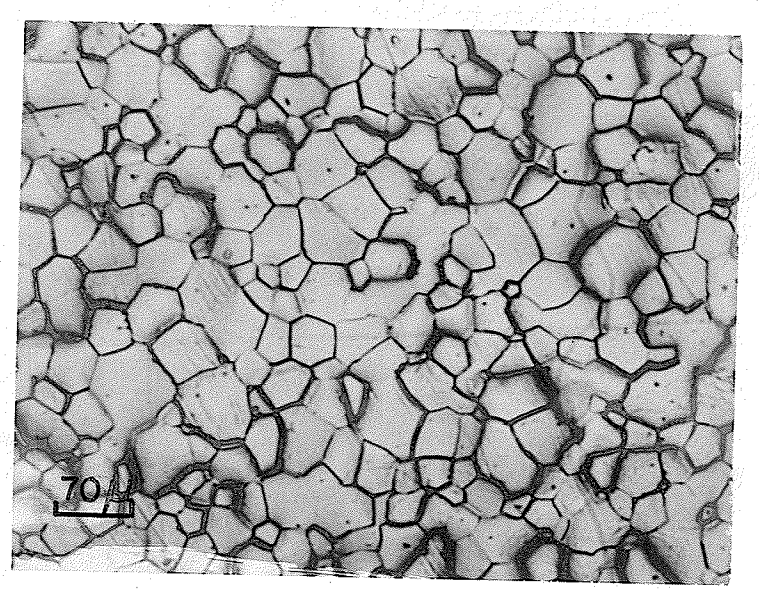

Figure 12 Typical micrograph of annealed MgO specimen showing some dislocation etch pits due to grown in dislocations.

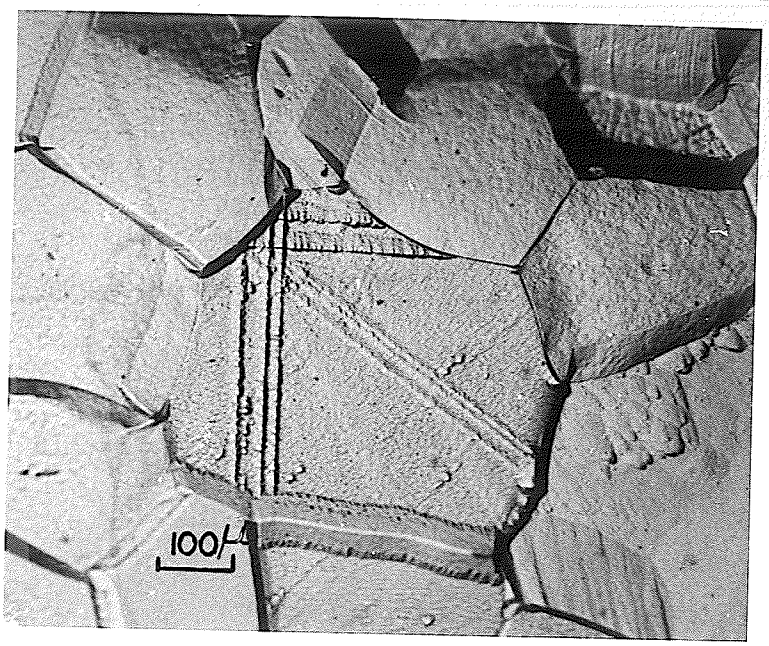

Figure 13 Slip initiation in MgO grains at the microyielding stress level.

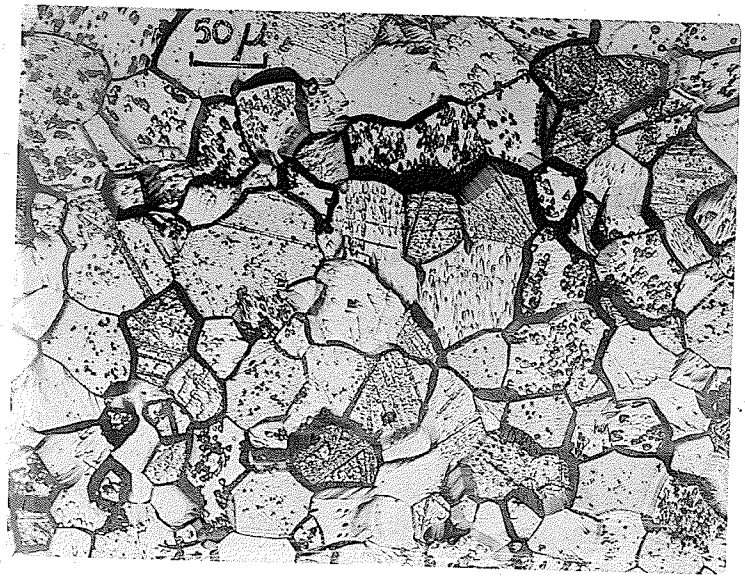

Figure 14 Slip activity in MgO grains far away from the cracks.

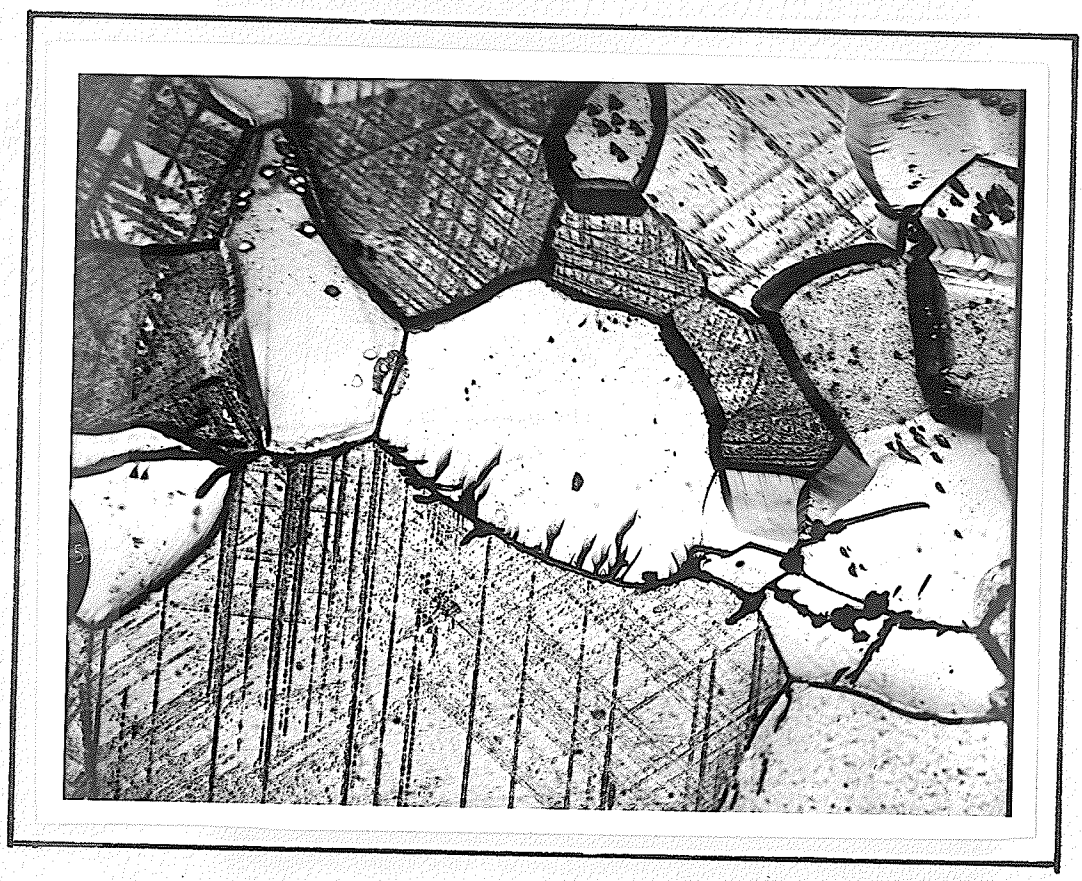

Fig. (15) Microcracks formed due to obstruction of slip bands at grain boundary. Notice that micro cracks appear at both sides. X 150.

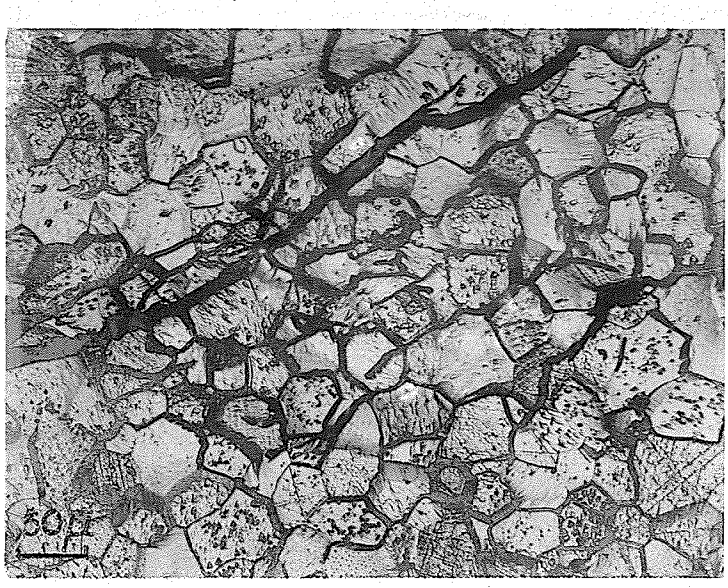

Figure 16 Micrograph showing transgranular cracks.

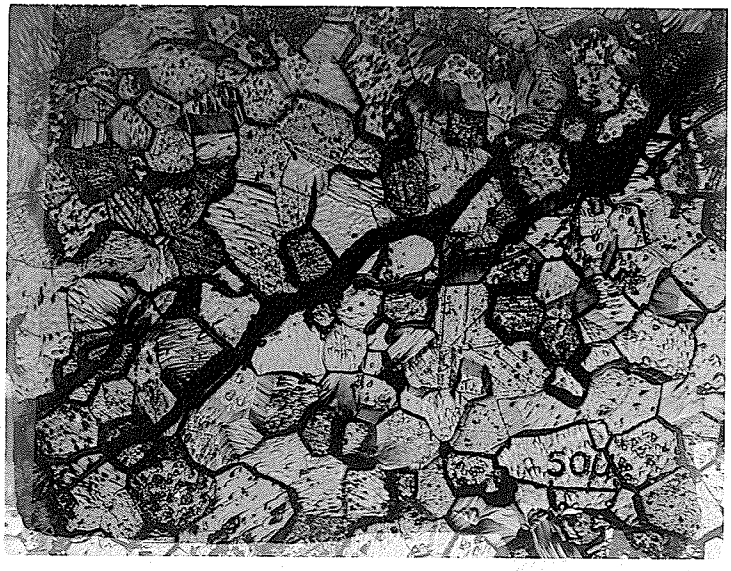

Figure 17 Micrograph showing an area surrounding a propagating crack.

Direction of crack propagation

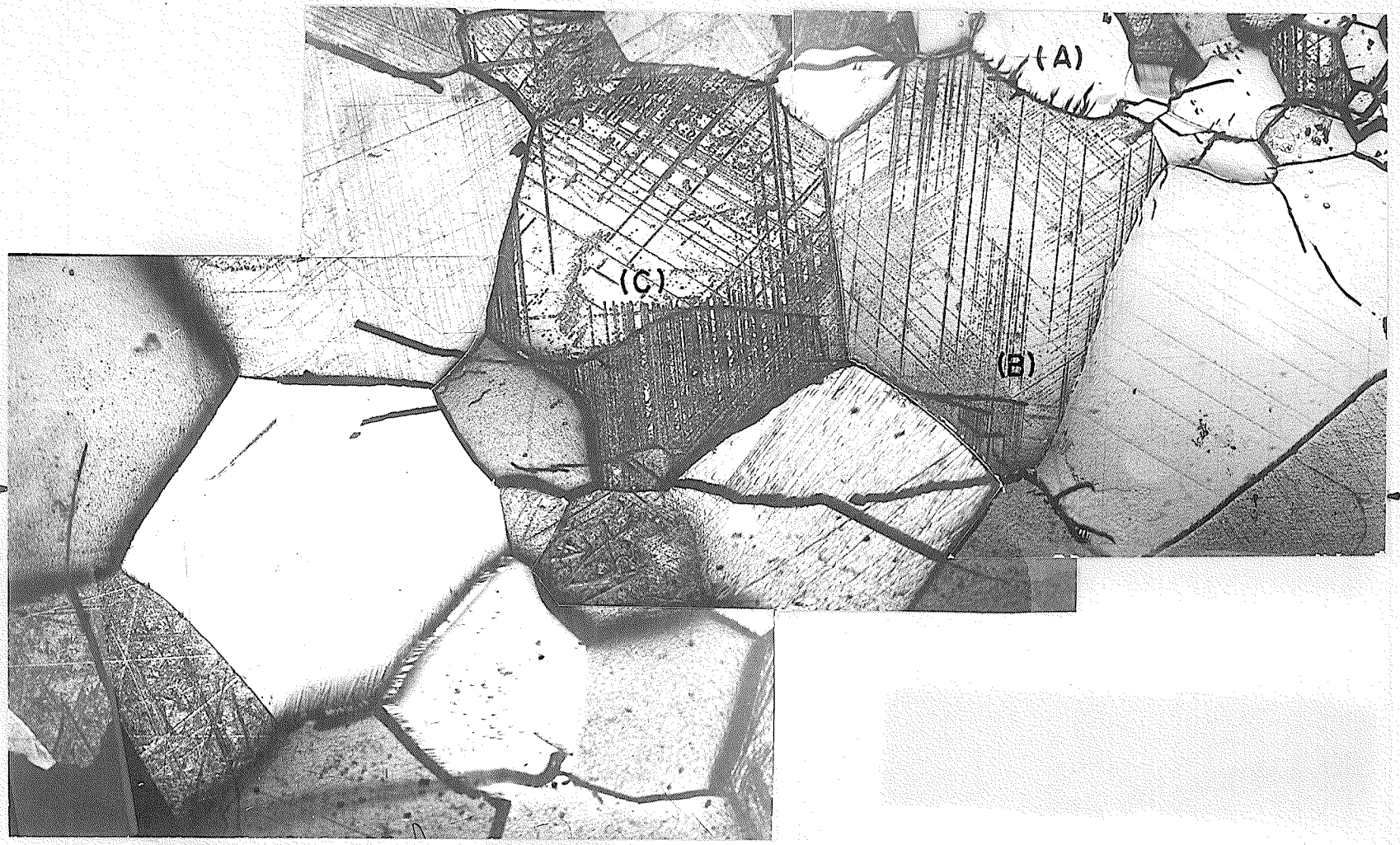

Loading direction

Fig.(18) Composite micrograph showing the microstructural features of polycrystalline MgO after compression. X 100

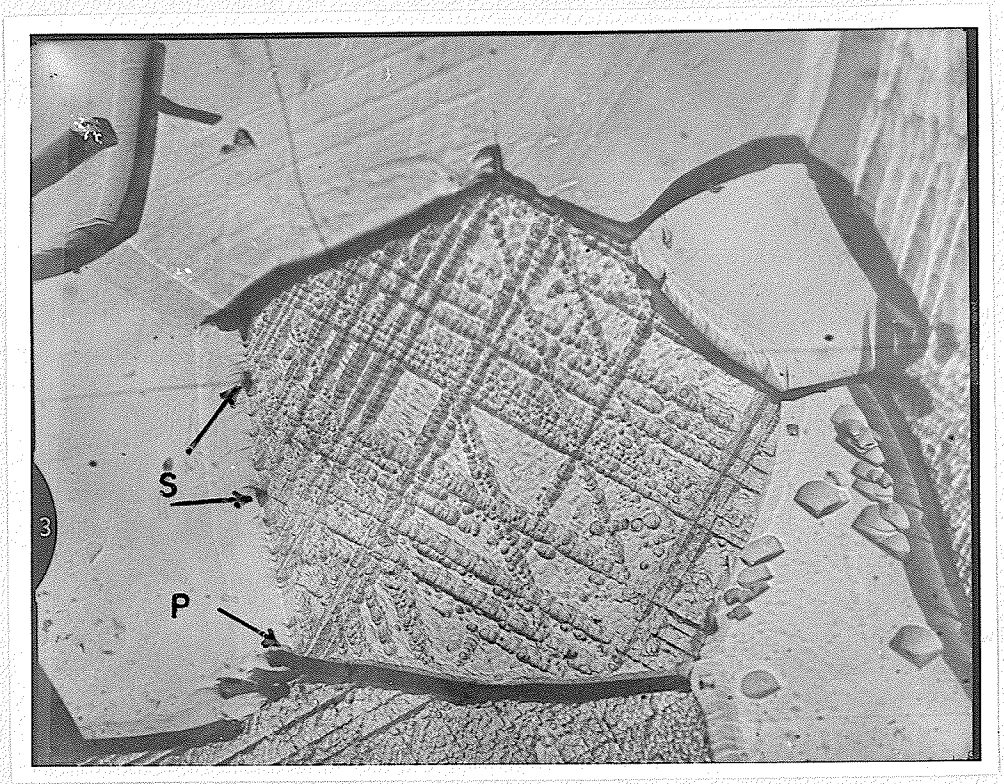

Fig. (19) Plastic deformation and formation of microcracks at the triple points "P" and at the intersection of slip band with the grain boundary "S" as revealed by etch pitting after deformation. x 185

seen in earlier work [33]. The same figure illustrates the formation of microcracks near the triple points and whenever a slip band is obstructed by a non-favourably oriented grain boundary. Figure (20) is an enlarged micrograph for a portion of the main crack at grain "c" of figure (18). It shows that the crack travels across the grain in steps parallel to the loading direction. Figure (21) shows the zone at the crack tip. It can be seen that there is an array of small-unjoined microcracks. The same figure illustrates that slip bands of different orientation are formed at the crack tip in order to dissipate part of the energy associated with the advancing crack. Figure (22) shows the branching of a main crack as it travels in the material.

Based on the microstructural studies the following observations are summarized:

1. Cracks extend in a direction parallel to the loading axis.
2. In compression, cracks propagate transgranularly.
3. The propagation of a crack is accompanied by extensive plastic deformation along the crack front together with the initiation of secondary cracks in some grains surrounding the crack.
4. Microcracks were observed to form in the following cases:
   - i. When a slip band is obstructed by an unfavourably oriented grain.
   - ii. When slip bands of different slip directions intersect.
   - iii. Near the triple points.

Direction of crack propagation

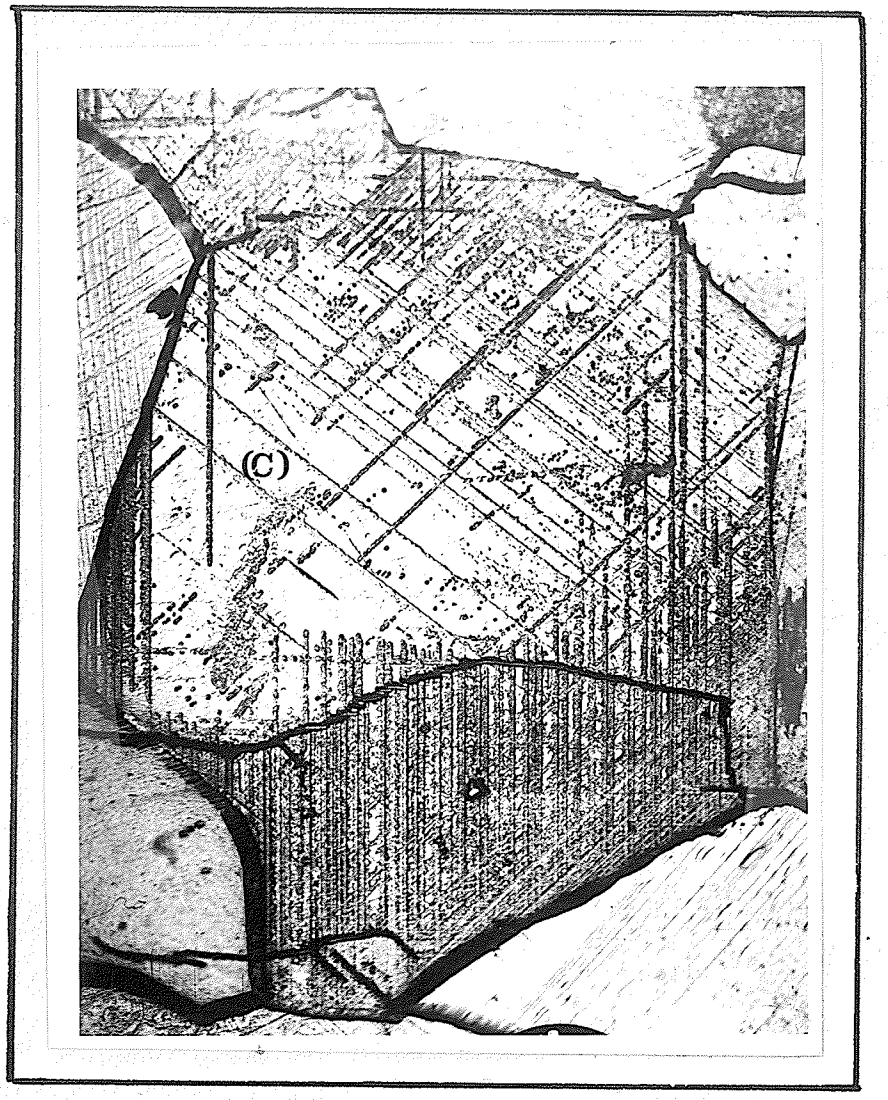

Fig.(20) Details of slip activity along the crack front travelling in grain 'C'.
X 180

Direction of crack propagation →

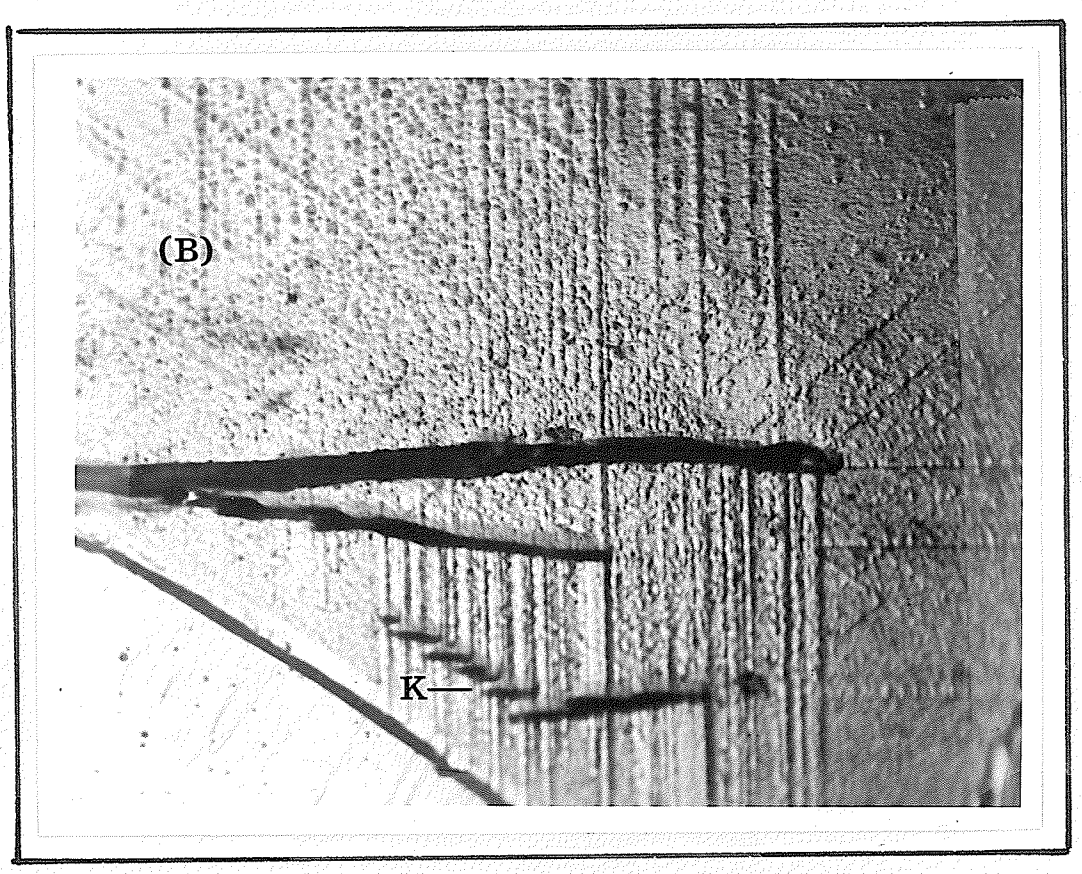

Fig. (21) Details of plastic deformation at the crack tip in grain 'B'. Notice the small microcracks 'K' and their direction. X 550.

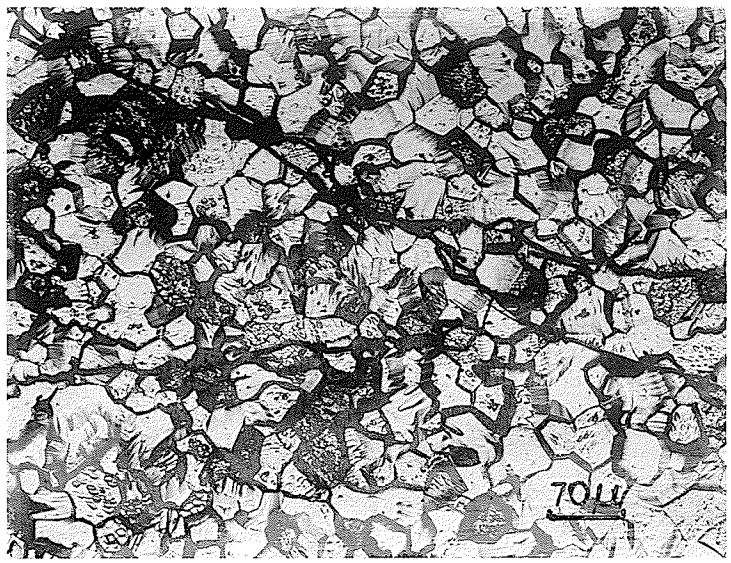

Figure 22 Typical micrograph showing the branching of the main crack.

4.3 Acoustic Emission Observations

Acoustic emission was monitored during all the compression tests performed during the course of this study. At different load levels, AE pulses were displayed on an oscilloscope screen. Figure (23) represents the oscilloscope traces of typical (AE) pulses monitored in the microplastic region, "stage 1". It can be seen that, the AE pulses have the low peak amplitudes. These signals are thought to be representing the microplastic region. Figure (24) shows the oscilloscope traces of AE pulses monitored in the macroplastic region as defined on figure (7). It can be seen that the AE pulses have, relatively, medium peak amplitudes. It is noted that the shape of the pulses indicate that their frequency is higher than those signals observed in the microplastic region. Figure (25) represents typical oscilloscope traces of AE signals monitored at stress levels higher than 50% of the fracture stress 'σ_f' and just before fracture. It can be seen that, the signals have very high peak amplitude. In this region, AE signals, are of the burst type. Those signals are thought to be representing microcracks initiation and cracks propagation. It should be mentioned that the gain was reduced to 73 dB during the loading range from 50% σ_f till the sample fractured to monitor the high amplitude signals without saturating the monitoring system.

Figure (26) is a plot of the load and total AE counts during the deformation of polycrystalline MgO under compression. It can be

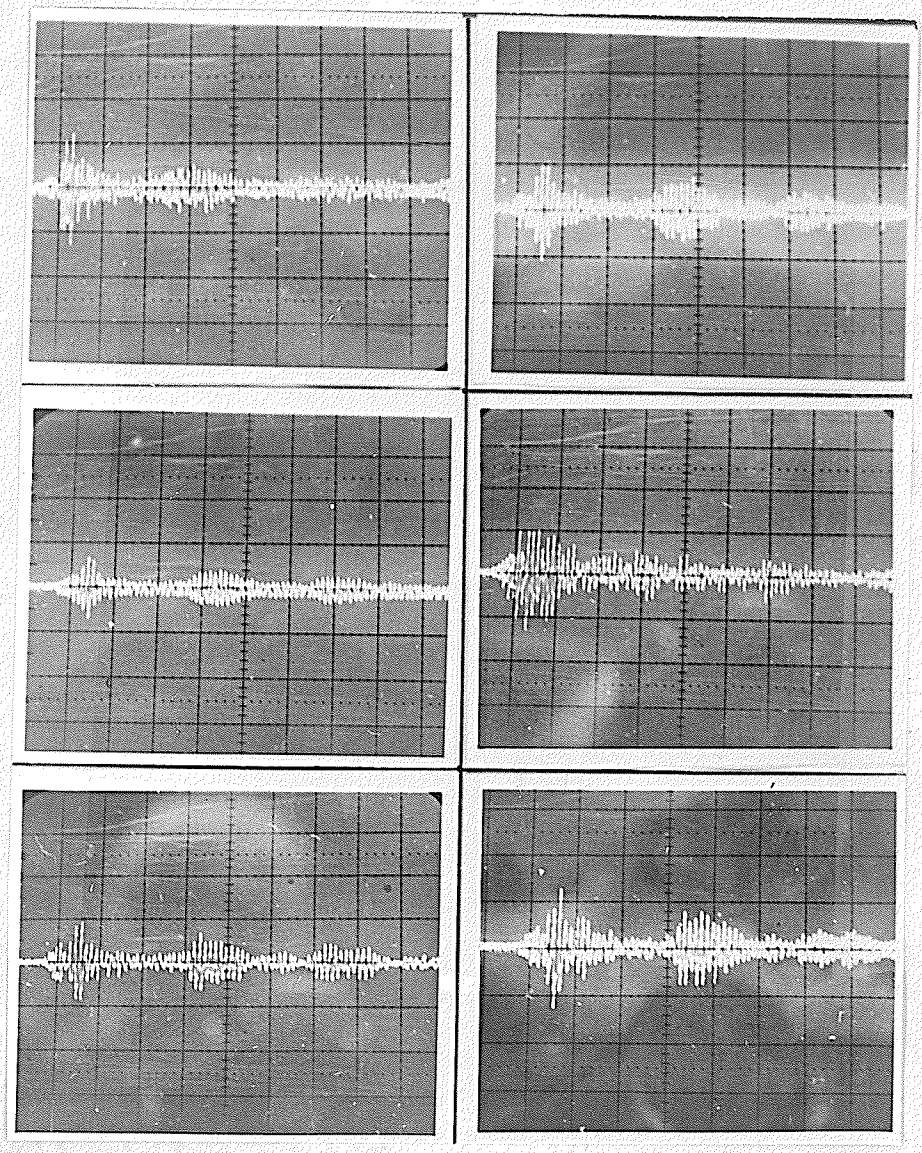

Figure 23 Oscilloscope traces of AE pulses in the microplastic region.

Abscissa - 50 μ seconds/division

Ordinate - 250 μ volt/division

Gain - 80 dB

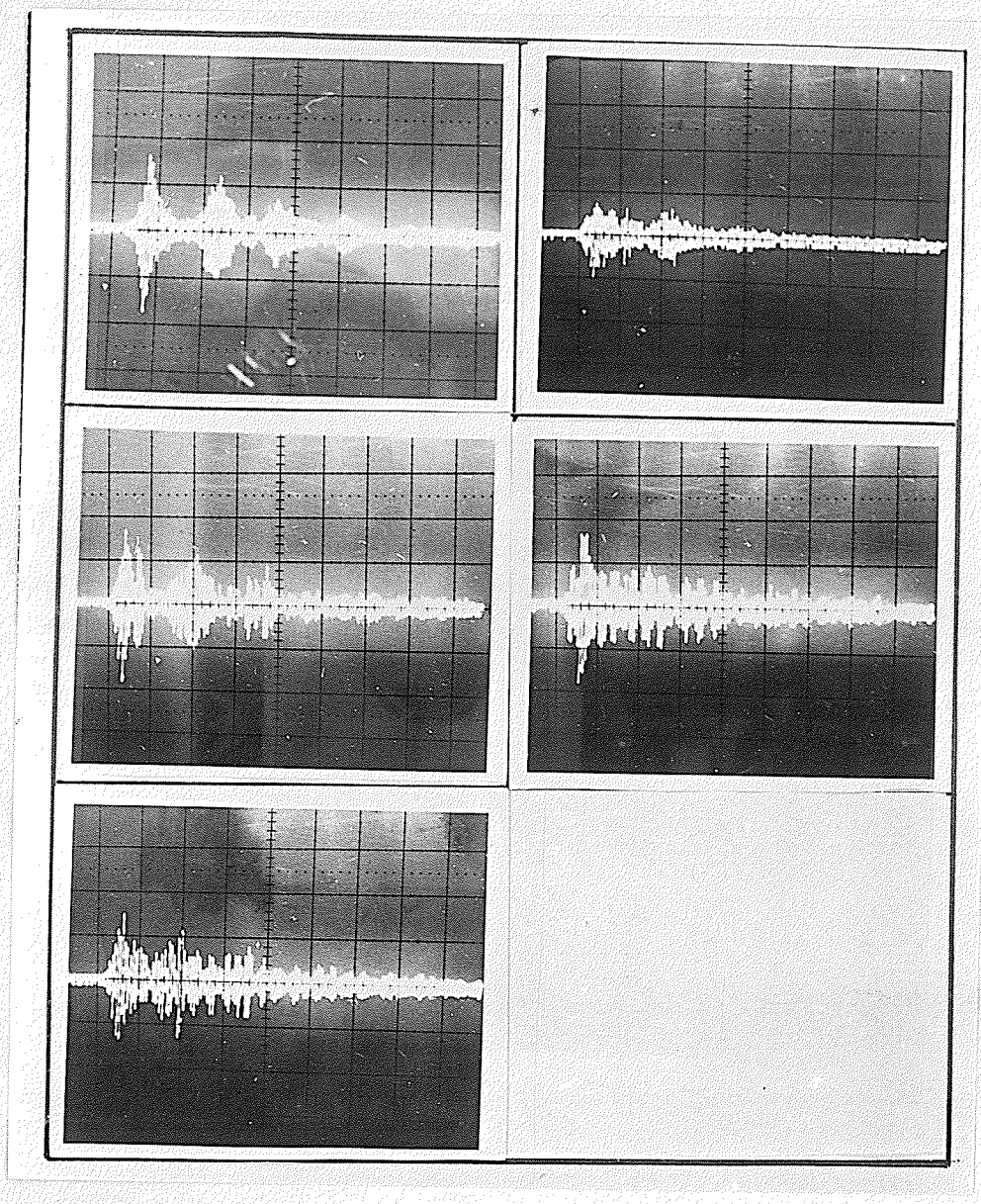

Figure 24 Oscilloscope traces of AE pulses monitored in the macroplastic region.

Abscissa 100 μ second/division

Ordinate = 250 μ volt/division

Gain 80 dB

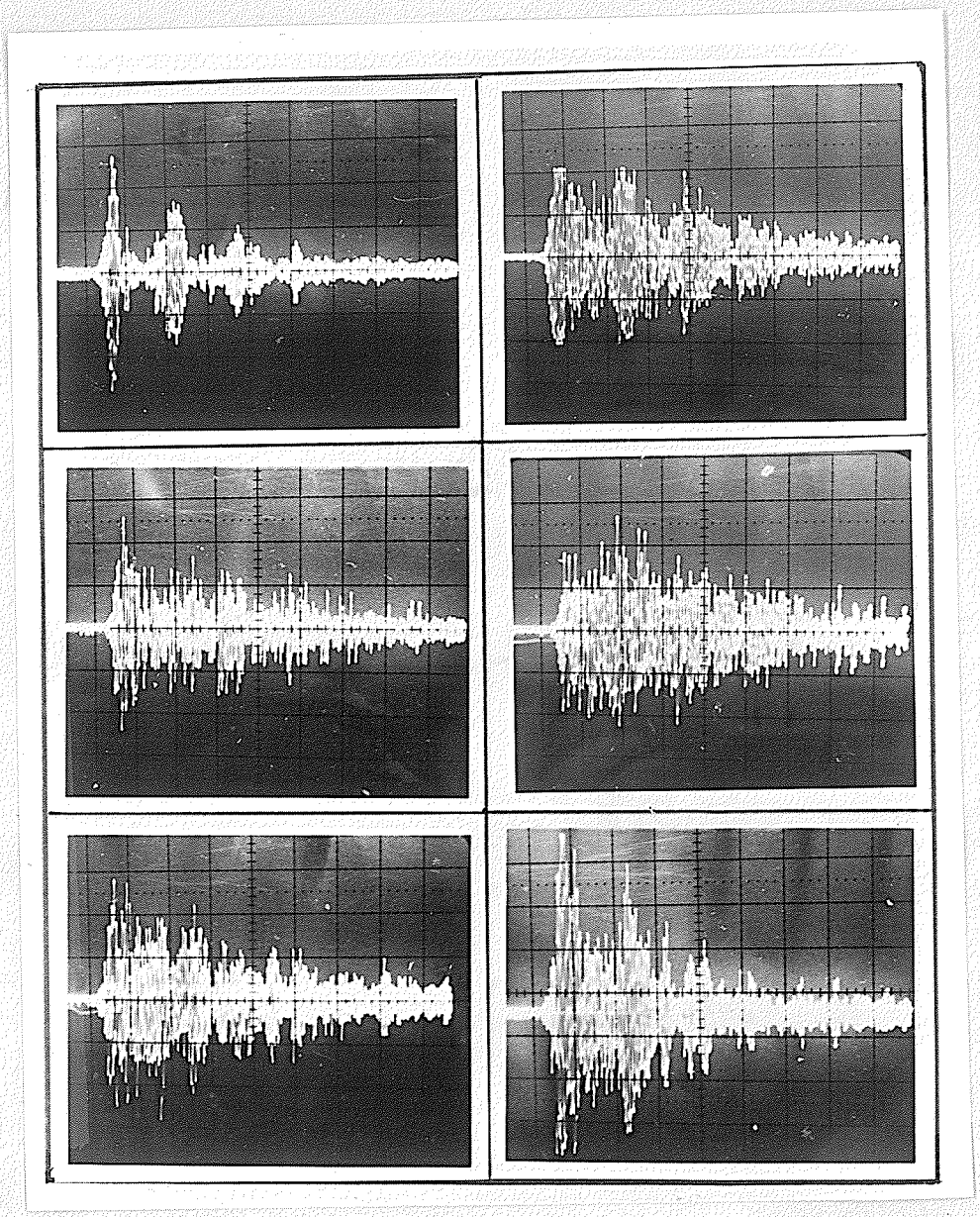

Figure 25 Oscilloscope traces of AE pulses observed at stress levels higher than 50% of the fracture stress.

Abscissa = 100 μ second/division

Ordinate = 559 μ volt/division

Gain = 73 dB

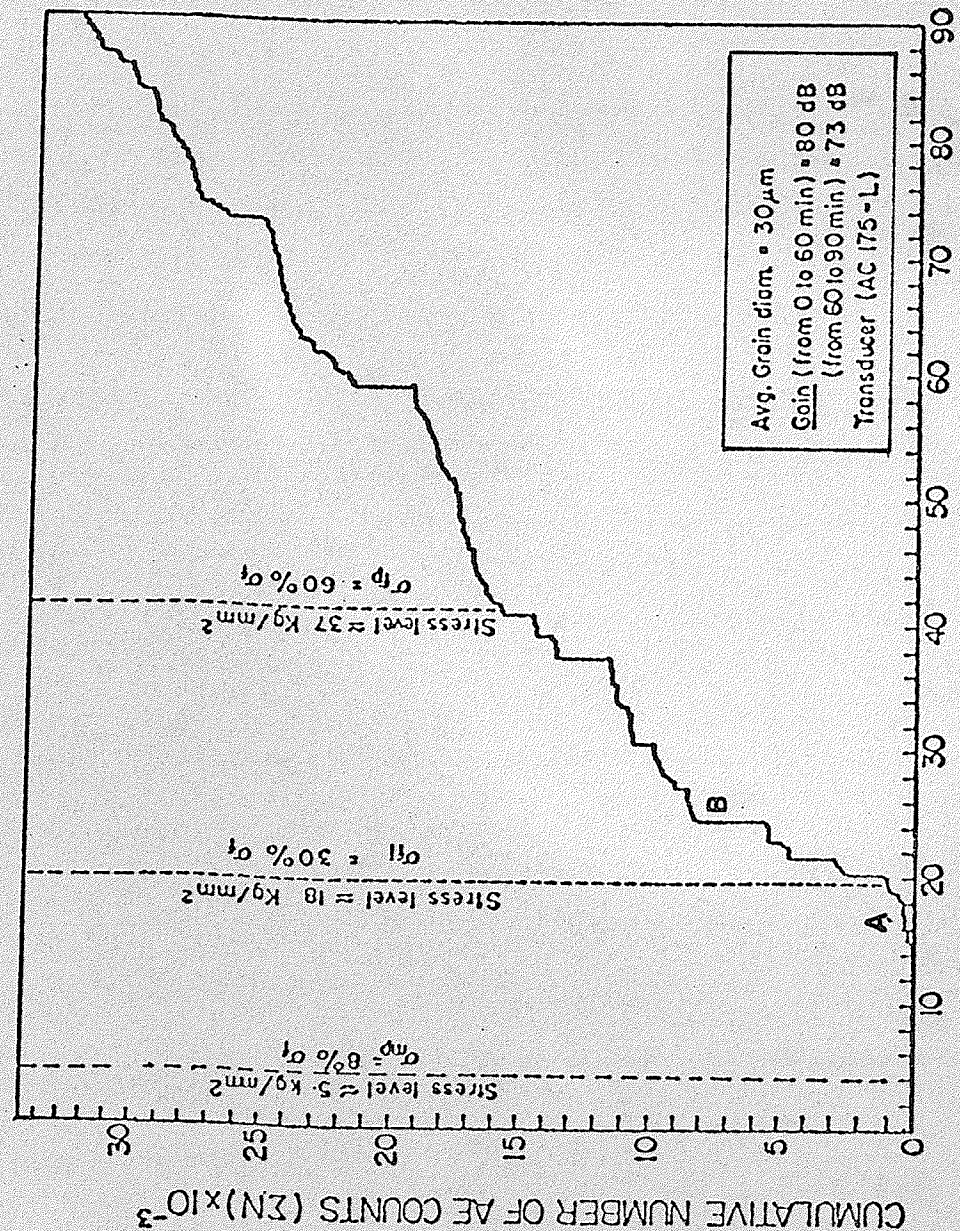

Fig.(28) Cumulative number of counts vs. time for MgO sample deformed in compression.

seen that, the total counts curve demonstrates two distinctive features. Firstly, the total number of counts increases in steps followed by short periods of inactivity as seen in region "A". This is likely to result from AE signals emitted during the plastic deformation of a brittle material. Secondly, the total AE curve shows sharp increases due to the emission of large number of AE signals as seen in region "B".

The computer was employed to process the load and AE data obtained during the compression tests. Figure (27) is a typical plot of the load and AE count rate per second. In the initial loading stage, a very small number of isolated counts was observed. As the load was increased, the acoustic emission rate showed a gradual increase in the count rate. As the load exceeded 50% of the fracture load, the AE count rate increases in the form of spikes, as the number of counts emitted due to crack propagation increases. From the figure, it can be seen that, the count rate shows a peak just before the failure of the specimen. Figure (28) is a plot of AE count rate and cumulative number of counts versus load. The figure shows that AE rate changes in an erratic manner in the early loading stage and reachs a maximum value near the complete failure of the specimen. Figure (29) is a plot of the cumulative number of AE counts up to fracture versus grain size. This figure shows that, at fracture stress, the total AE counts decreases as the grain size increase up to a critical grain size of about 105 microns. As for grain sizes larger than the critical value, the total

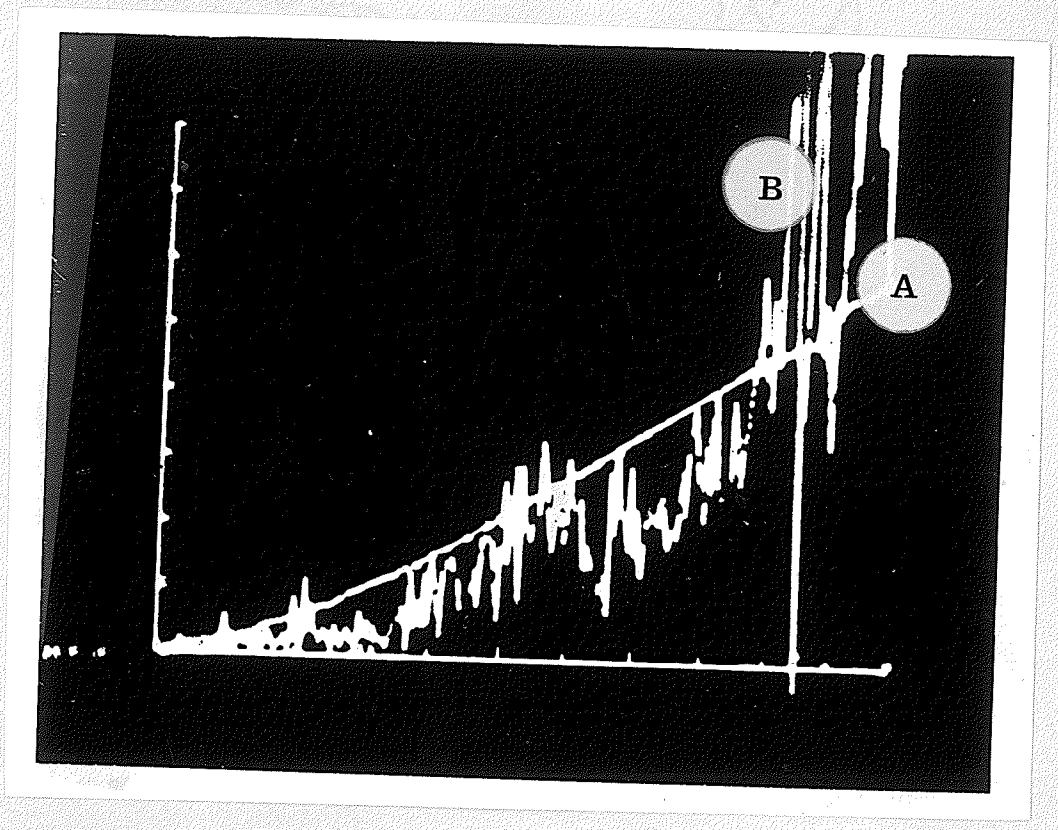

Figure 27 Computer plot of load (A) and AE count rate (B) for 200 microns main size polycrystalline MgO.

Abscissa = 22 seconds/division

Ordinate:

Load = 125 kg/division

AE count rate = 60 counts/second

Gain = 76 dB

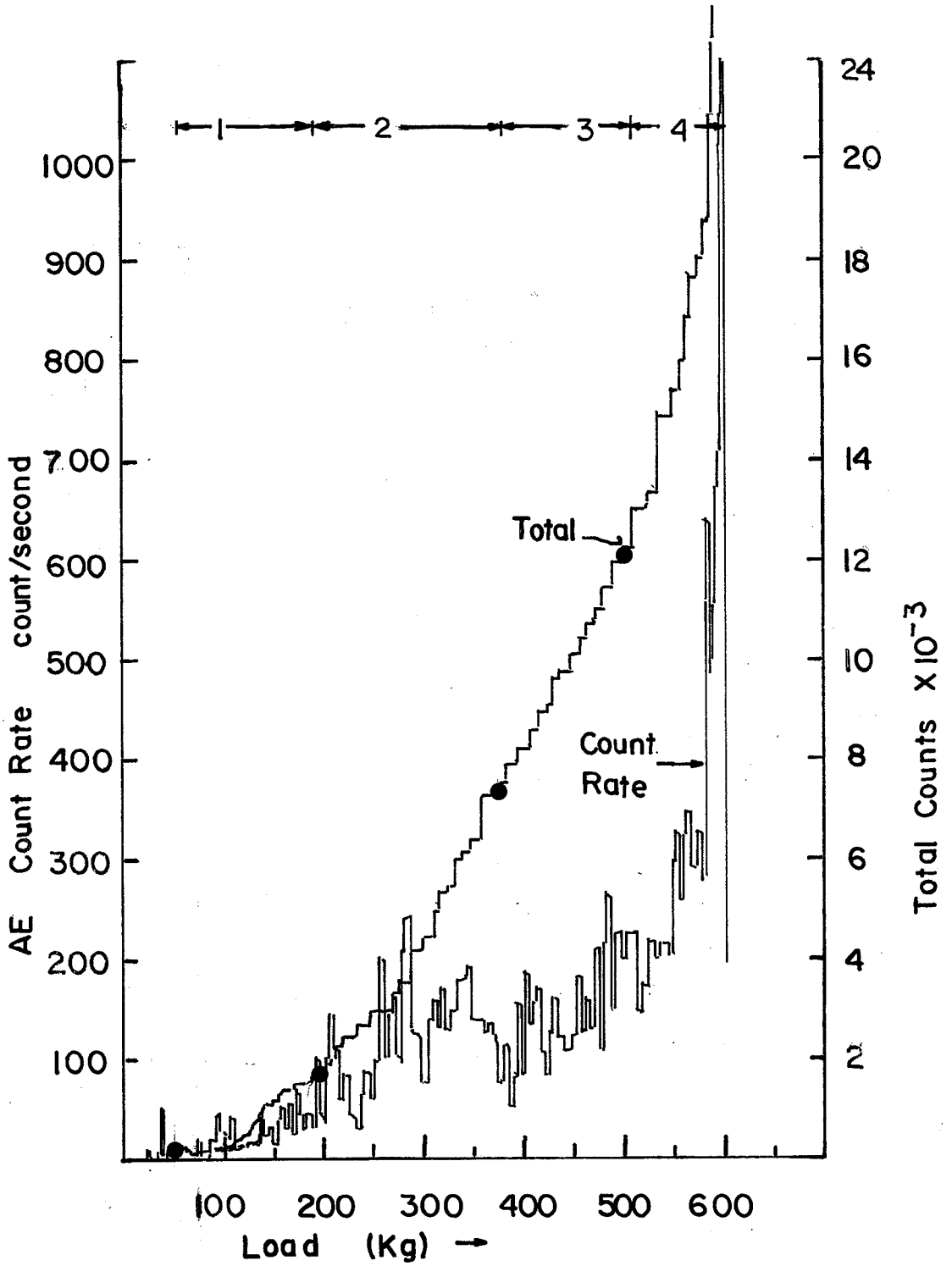

Fig.(28) AE Count rate and total counts vs. load during the deformation of 200 micron grain size.

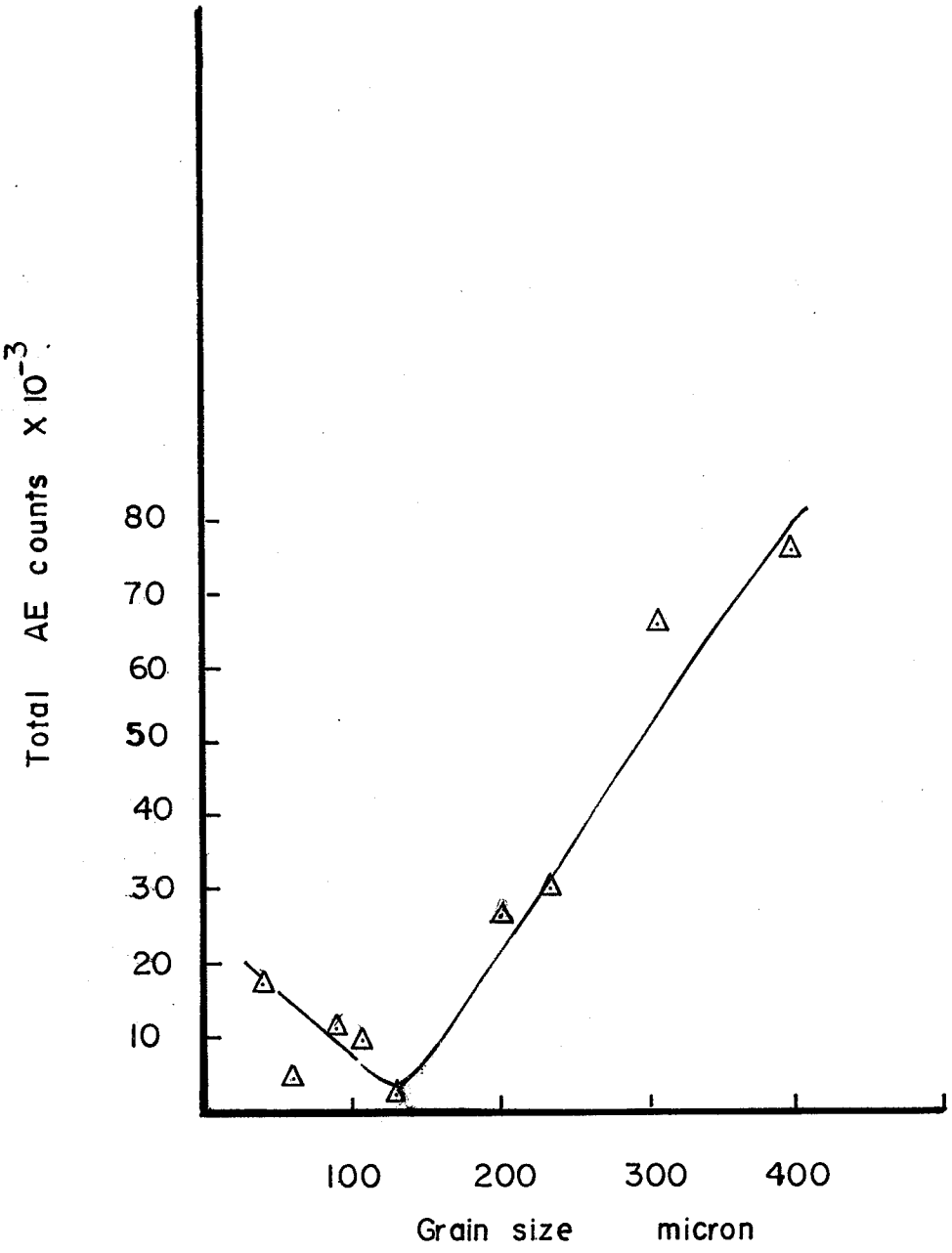

Fig. 29 Cumulative total AE events for polycrystalline MgO at fracture.
Gain = 76 db
Filter = 50—500 Khz

AE counts increases as the grain size increases.

Based on the results of AE monitoring during the deformation of polycrystalline MgO under compression, the following observations are made:

1. Few AE counts appear in the microplastic stage with some periods of inactivity.
2. The increase in the total AE counts takes two forms; firstly, in the form of short steps due to the emission of less frequent AE pulses which accompany the plastic deformation and secondly, sharp increases or jumps due to the emission of large number of counts which are likely to accompany cracking.
3. Three different types of signals are observed during the deformation of polycrystalline MgO; firstly, a very low amplitude signal which occurs in the microplastic region, secondly, medium amplitude signal which is thought to characterize microcrack formation and thirdly, signals with very high peak amplitude and relatively high frequency which appeared before the sample fractures.

CHAPTER V

DISCUSSION OF RESULTS

The compression tests described in the previous chapter have generated information about two topics; a) the use of AE to monitor and characterize the behavior of polycrystalline MgO at ambient temperature, and b) the effect of microstructure on the fracture stress of specimens with different grain size. These topics are discussed as follows: section (1) considers various energy dissipating processes responsible for acoustic emission activity, section (2) considers the effect of grain size on the fracture stress, and section (3) consider a correlation between the cumulative AE total counts and the magnitude of strain.

5.1 Energy dissipating processes responsible for AE.

Acoustic emission activity observed during the compression of MgO samples can be attributed to: (a) initial loading and seating of the specimen, (b) localized plastic deformation in favorably oriented grains, (c) microcrack initiation, (d) macrocrack propagation and (e) catastrophic failure.

5.1.1 Initial loading and seating stage.

In this case, the basic sources of AE are: the mechanical adjustment between the specimen and the grips and the frictional effects resulting at the interface between the grips and the specimen during loading. According to the data obtained in this investigation, the initial loading and seating stage extended from 0 to $\sim$ 8% of the fracture stress level. However, it has been found that by using a suitable lubricant (silicon lubricant), the frictional effects are minimized. This aspect is clear from figure (26), where negligible number of counts was observed in the early loading stage. The acoustic

emission, in this stage is mostly of very low peak amplitude and consequently, they are not expected to trigger the counter; and therefore unlikely to affect the AE measurements.

5.1.2 Plastic deformation.

Plastic deformation results in intense AE if the dislocations generate in the form of discrete glide packets [36]. This happens only in the microplastic stage when new dislocation sources are being activated. Thus, the strain increment which results from the generation of dislocations, can result in observable acoustic emission [37]. The generation of grain boundary dislocation sources has been established by Sinha et al [33] as the mechanism responsible for microplasticity in polycrystalline MgO.

In the present data, the localized slip associated with dislocation activity at grain boundaries is clearly shown in figure (13). The microyield stage extended from a stress level of ≃ 8% up to 30% σ_f, where small number of AE counts, (figure 26) associated with low peak amplitude (figure 23) are observed. This observation together with the microstructural observations of figure (13), suggests that most of AE activity in this stage is due to generation of dislocations from grain boundaries and formation of localized slip bands. This is generally in agreement with the observations of Liptai et al [2] on flaw free samples of brittle materials.

5.1.3 Microcrack initiation and slip initiation.

In randomly oriented polycrystalline aggregate two processes are likely to occur simultaneously; these are: slip initiation and

microcrack initiation. The microstructural data of figure (18) clearly show that the two processes are taking place. The data show that the obstruction of slip bands at the grain boundary has resulted in slip initiation in the neighboring grain if it is favorably oriented. Thus, the stress concentration at the tip of the slip bands are relaxed and this relaxation is accompanied by the emission of AE signals. These signals are typically of low peak amplitude. On the other hand, microcrack initiation occurs if the neighboring grains can not accomodate the plastic shear strain accompanying the movement of a large group of dislocations [35]. This situation arises when a slip band is obstructed at the grain boundary. Following the work of Tetelman and Chow [38], the condition for a microcrack initiation is:

$$T_N\, nb = T_i\, nb + 2\gamma$$

where: T_N = critical shear stress required to initiate a crack

T_i = frictional stress opposing the motion of dislocation

n = number of dislocations in a slip band

b = Burger's vector

γ = total elastic plus plastic work per unit area expended in making microcrack surface area.

To elaborate on the condition of microcrack initiation, consider a slip band which is obstructed at the grain boundary. A stress field is likely to develop at the tip of the slip band if no plasticity has taken place in the neighbouring grain. Thus a microcrack is initiated when the local stress field equals to or exceeds

the decohesive stress of the material. The initiation of a microcrack results in rapid release of energy and the emission of large number of AE signals. This is clearly seen from the jumps in the total number of AE counts shown in figure (26). This behavior was commonly observed in the range of ≃ 30% to ≃ 60% σ_f.

The AE activity observed in this stage is mainly due to both slip and microcrack initiation. Oscilloscope traces of AE pulses in this stage clearly illustrate this behavior. Figure (24) shows the two types of signals observed in this stage. However, it should be noted that the clear distinction between the two types of signals is difficult. Thus, we propose that the relatively low amplitude signals (similar to those observed in the microplastic stage) are characteristic of plastic deformation, while the high amplitude signals are characteristic of crack initiation.

5.1.4 Propagation of cracks.

Microcracks which are initiated by the obstruction of slip bands at the grain boundary will not propagate unless the energy input, supplied by the external stress, exceeds the energy required to extend the crack. As the external stress is increased, the energy condition is satisfied and the crack extends. The extension of a crack is generally associated with various energy dissipating processes such as, plastic deformation, formation of small unjoined cracks in the grains surrounding the main crack, similar to those observed in figure (21), formation of microcracks and branching of the main crack as observed in figures (18) and (22) respectively. Thus, the energy available for the extension

of the crack drops and the external stress has to be increased again to extend the crack further. In other words, this stage is characterized by stable propagation of cracks, since the propagation is controlled by the increase of the external stress.

The propagation of a crack results in the emission of large number of AE signals. The AE activity in this stage is characterized by the presence of three different signals: a) a low amplitude signal similar to that observed in the microplastic stage and is due to the heavy plastic deformation accompanying the propagation of the crack, b) a high amplitude signal similar to that observed in the macroplastic stage and characterizes the crack initiation, and c) a medium amplitude signal which is proposed to be due to the propagation of cracks. It should be noted that this stage was commonly observed in the range of $\simeq$ 60% to 90% σ_f.

5.1.5 Catastrophic failure

Final fracture of the entire specimen occurs when the load bearing areas of the specimen can not withstand the applied stress. Then, the complete separation of the material takes place and failure of the structure occurs. The collapse of the specimen is accompanied by an intense AE activity associated with very high peak amplitude signals. The AE events occur rapidly producing a peak in the AE count rate.

A summary for the interpretation of AE data in terms of the microstructural observations is shown in figure (30).

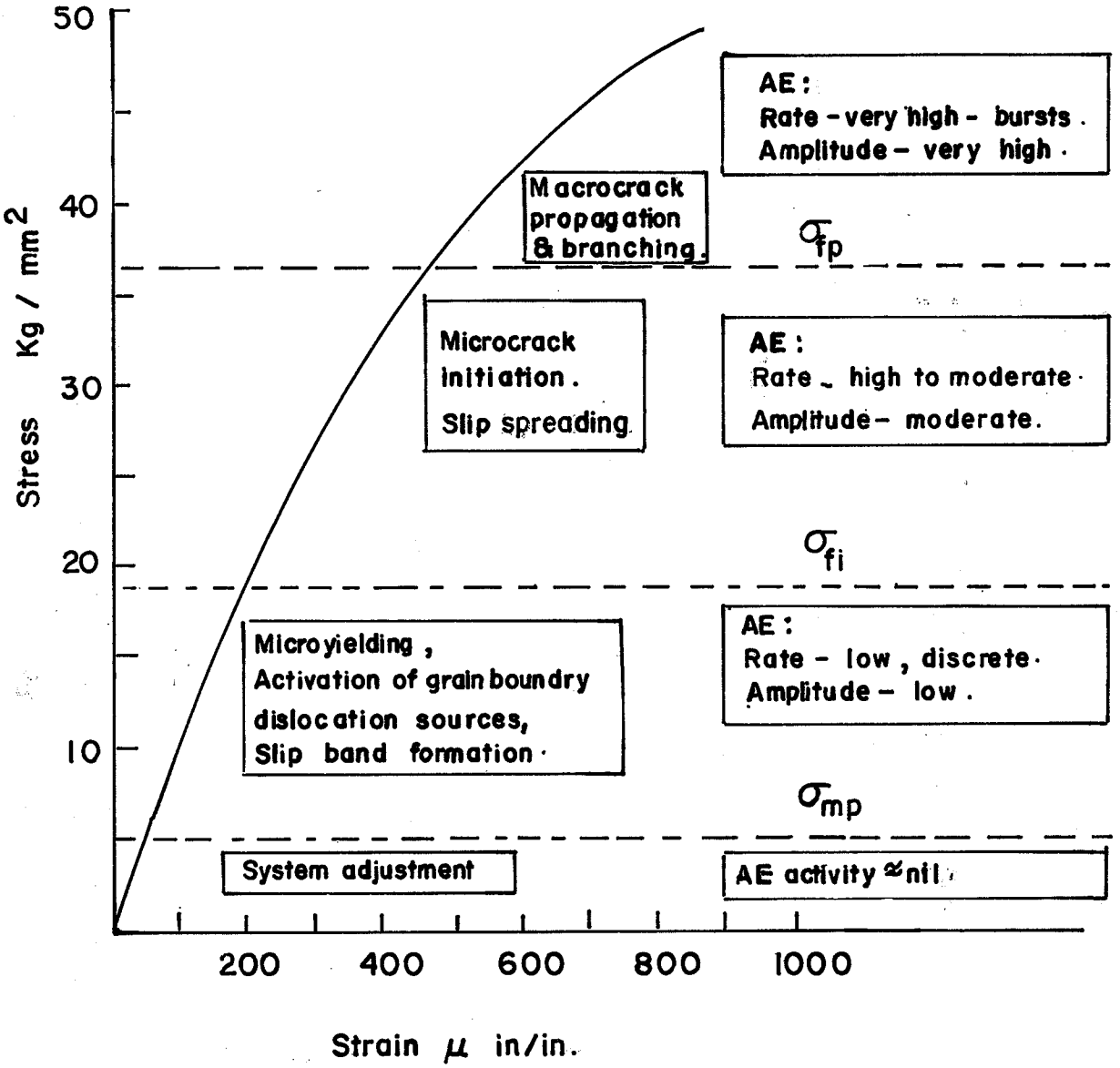

Fig. (30) Summary of AE data and microstructural observations during the deformation of polycrystalline MgO under compression.

5.2 Grain Size and fracture stress.

The macroscopic response of polycrystalline MgO under unaxial compression has shown that both the total strain and the fracture stress exhibit a non linear behavior with the increase of D (Fig. (8)) and $D^{-1/2}$ (Fig. (10)) respectively.

The effect of the grain size on the total strain may be explained as follows: as the grain size decreases, the surface area of the grain boundaries per unit volume of the material increases. Thus, more grain boundary dislocation sources are likely to generate dislocations as the external stress increases. In other words, more energy is expended in slip initiation in favorably oriented grains, therefore, crack initiation is likely to be restricted in fine grain size materials. Figure (9), shows that the fracture stress increases as the grain size decreases. This behavior may be explained as follows: the magnitude of the stress concentration at the tip of a slip band is controlled by the size of grain boundary ledges which in turn increases as the grain size increases [19]. Thus, it is expected that, the magnitude of stress concentrations at grain boundary ledges in fine grain specimen will be less than those generated in coarse grain specimens which explains the observation that fine grain size specimens fracture at high stresses. As for coarse grain size specimens, the magnitude of the stress concentration are likely to initiate cracks rather than plastic deformation and the specimen fractures at relatively low stresses.

The non-linear behaviour of σ_f vs. $D^{-1/2}$ may be explained by following Ibrahim and Tangri's model for the fracture of un-irradiated samples of MgO deformed under uniaxial tension [35]. In this model, the slope of σ_f versus $D^{-1/2}$ was proposed to be dependent upon grain size as follows:

$$\sigma_f \simeq \sigma_{oF} + \alpha(6\pi G)^{1/2} (\gamma_s + \gamma_{irr}^{(D)})^{1/2} D^{-1/2}$$

where σ_{oF} is an initial fracture stress, α is a geometrical factor, G is the shear modulus, γ_s is the reversible component of the surface energy and $\gamma_{irr}^{(D)}$ is the irreversible component of the surface energy.

The irreversible component $\gamma_{irr}^{(D)}$ accounts for various irreversible energy dissipating processes associated with crack propagation; namely, plastic deformation, microcrack formation, and secondary crack formation.

In the present study, fig. 8 shows that the amount of strain-to-fracture is dependent upon grain size, in a manner similar to that observed by Ibrahim and Tangri[35]. Thus it may be concluded that the observed non-linearity in σ_f vs. $D^{-1/2}$ is due to the dependence of the term γ_{irr}^{D} on grain size.

5.3 Acoustic emission and deformation

For the purpose of understanding the relationship of AE and deformation, an attempt was made to correlate the cumulative number of AE events and strain. The result of this correlation is shown

in figure (31). From figure (31-A), it is observed that the data suggest an exponential relationship between the total number of events and strain. This relationship was assumed to take the form:

$$\Sigma\phi = Q \cdot \varepsilon^{A}$$

where $\Sigma\phi$ = cumulative number of AE events

ε = strain min/in

Q and A = numerical constants

This assumption was verified by plotting $\Sigma\phi$ versus strain on the log-log scale as seen in figure (31-B). It can be seen that the resulting straight lines exhibit changes in their slope at certain load levels (marked on figure 31-A). These levels were found to be at $\simeq$ 10% σ_f, 33% σ_f, 62% σ_f and 92% σ_f. Those levels were found to be consistent with the microstructural changes revealed by etch pitting and used to identify the three deformation stages, namely; the microplastic, macroplastic and fracture regions (figure 7).

A computer program was used to analyze the data and the following numerical expressions were found:

$$\phi_1 = 3.6992 \times 10^{7} \varepsilon^{1.1658} \qquad 5.3.1$$

$$\phi_2 = 1.8448 \times 10^{11} \varepsilon^{2.1688} \qquad 5.3.2$$

$$\phi_3 = 1.7635 \times 10^{12} \varepsilon^{2.4596} \qquad 5.3.3$$

where ϕ_1, ϕ_2 and ϕ_3 are the cumulative number of AE events in the following regions ($\simeq$ 10 to 33% σ_f), (33 to 62% σ_f) and (60 to 92% σ_f).

To cross check, equations (5.3.1), (5.3.2) and (5.3.3) were differentiated with respect to time. The count rates were determined for strain values in the microplastic, macroplastic and fracture regions respectively. The results of this cross check showed reasonable agreement with the AE count rate as displayed by the computer during the play back of data tapes.

The numerical values of A and Q were found to differ from one grain size to another. Thus, further studies on the effect of grain size on the AE behavior are needed in order to elucidate the physical significance of these constants.

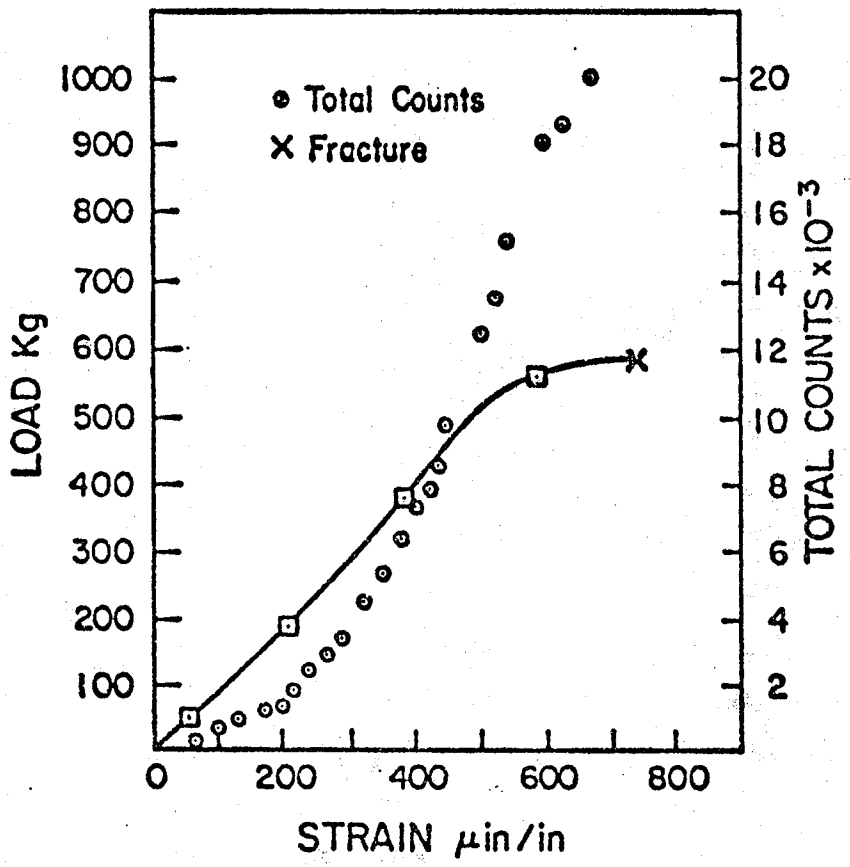

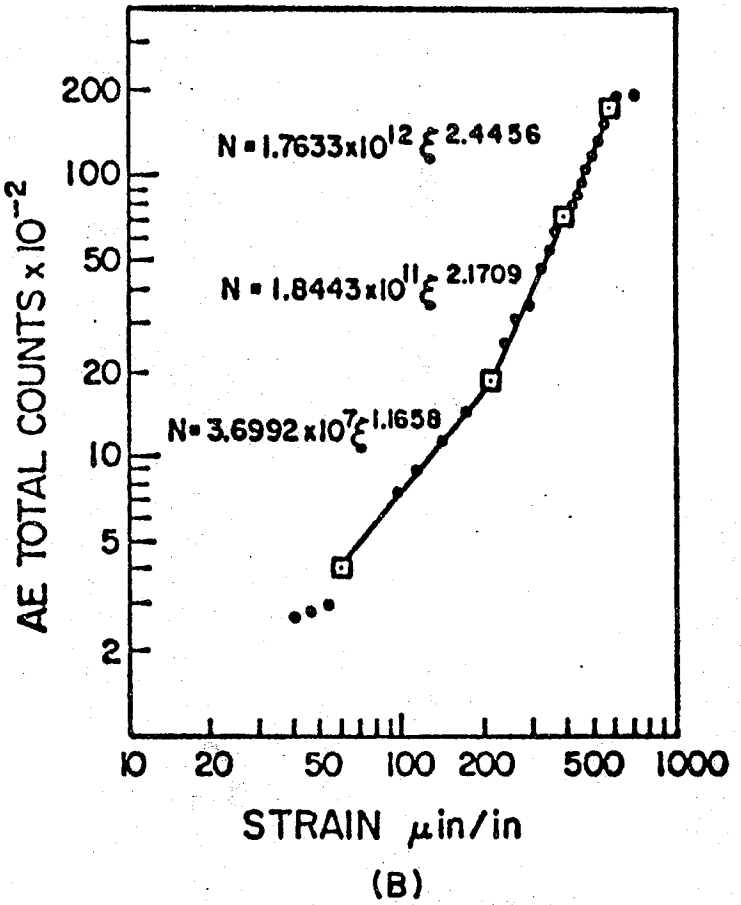

Fig. (31) Number of AE counts and load vs strain for 200 micron grain size polycrystalline MgO. Strain rate 10^{-4} second^{-1} ; Gain 76 dB ; Filter = 50 - 500 KHz.

CHAPTER VI

CONCLUSIONS

AE data, confirmed by microstructural observations have led to the formulation of the following conclusions:

1. The stress-strain response under compression of polycrystalline MgO exhibits three stages of deformation:

   The first stage (microplastic stage), extends from $\sim$ 0.1 to 0.3 σ_f and is characterized by the generation of dislocations from grain boundary sources and the formation of localized slip bands in isolated regions in the grains. AE activity in this stage is characterized by a low amplitude signal associated with low count rate.

   The second stage (macroplastic stage) extends from $\sim$ 0.3 to $\sim$ 0.6 σ_f and is characterized by two microstructural features, a) intense slip bands and slip activity in favorably oriented grains, and b) microcracks at the regions of interaction between slip bands and unfavorably oriented grains. AE activity in this stage is characterized by two signals; a low peak amplitude signal similar to that observed in the microplastic stage and a high amplitude signal which, we propose, is due to the formation of microcracks.

   The third stage (fracture stage) extends from $\sim$ 0.6 to 0.9 σ_f and is characterized by stable propagation of cracks in the material. The propagation of cracks is associated with three important energy dissipating processes; namely, plastic deformation, formation of discrete unjoined microcracks and branching of the main crack. The AE activity in this stage is characterized by

the presence of three different signals: a) a low amplitude signal similar to those observed in the first stage, b) a high amplitude signal similar to that observed in the second stage, and c) a medium amplitude signal which, we propose to be due to the propagation of cracks.

2. A non linear behavior between σ_f and $D^{-1/2}$ is observed. This behavior is explained in terms of the dependence of effective surface energy on grain size in polycrystalline MgO.
3. The relationship between cumulative number of events and strain follows an equation of the form:

$$\Sigma\dot{\phi} = Q \cdot \varepsilon^{A}$$

where Q, A are constants within each stage of deformation but vary from stage to stage.

CHAPTER VII

RECOMMENDATIONS FOR FUTURE WORK

1. Further AE studies on the effect of impurities and second phase particles are needed. These studies are expected to be of technological importance, since the addition of second phase particles was found to play an important role in the fracture toughness of MgO.
2. Studies on the effect of the surface condition on the AE of the material are needed.
3. Further effort should be directed to study the effect of strain rate and temperature on the characteristics of AE activity obtained under uniaxial loading.
4. Further studies on the effect of grain size on AE behavior are needed.
5. Because of the limited resolution attained by optical microscopy, electron microscopy may be used as a better technique to study the microstructure.

List of References

[1] Pollock, A.A., "Acoustic Emission from Solids Undergoing Deformation", Ph.D. Thesis, University of London, 1970.

[2] Liptai, R.G., Harris, O.D., Engle, R.B. and Tatro, C.A., "Acoustic Emission Techniques in Materials", International Journal of Non Destructive Testing (3), 1971, pp. 163-217.

[3] Bill, R.C., "An Acoustic emission study of The Deformation Mechanisms of Polycrystalline Aluminum and Copper", Ph.D. Thesis, University of Michigan, 1970.

[4] Dunegan, H.L. and Tatro, C.A., "Acoustic Emission Effects During Mechanical Deformation", Techniques of Metals Research Volume V part 2, edited by R.F. Bunshah, (1973), pp. 273-279.

[5] Bellosillo, S.B., "Canadian Research and Development", May-June 1972, pp. 2-3.

[6] Schofield, B.H., "Acoustic Emission Under Applied Stress", ARL 150, Ad 274-484 Report, 1961, Office of Aerospace Research, U.S.A. Air force, p. 33.

[7] Ibid ....., p. 30.

[8] Dunegan, H.L., Harris, D.O. and Tatro, C.A., "Fracture Analysis By Use of Acoustic Emission", Engineering Fracture Mechanics, 1968, vol. 1, pp. 105-122.

[9] Dunegan, H.L. and Tatro, C.A., "Acoustic Emission Effects During Mechanical Deformation", Techniques of Metals Research, vol. V pt. 2, edited by R.F. Bunshah, p. 297.

[10] Ibid ....., p. 300.

[11] Fisher, R.M. and Lally, J.S., "Microplasticity Detected by an Acoustic Technique", Canadian Journal of Physics, 45, (1967), p. 1157.

[12] Thill, R.E., "Acoustic Methods for Monitoring Failure in Rock", New Horizons in Rock Mechanics, proceedings: 14th Symposium on Rock Mechanics held at Pennsylvania State University, June 11-14, 1972 By American Society of Civil Engineers, p. 649.

[13] Bieniawski, Z.T., "Mechanisms of Brittle Fracture of Rock", part 1 - Theory of The Fracture Process, Int. J. Rock Mech. Min. Sciences Vol. 4, (1967), pp. 404.

[14] Thill, R.E., "Acoustic Methods for Monitoring Failure in Rock", New Horizons in Rock Mechanics, Proc.; 14th Symp. on Rock Mechanics held at Pen. State Univ., June 11-14, (1972), pp. 659-687.

[15] Noone, M.J., Mehan, R.L., "Observation of Crack Propagation in Polycrystalline Ceramics and Its Relationship to Acoustic Emission", Fracture Mechanics of Ceramics, vol. 1, edited by R.C. Bradt, D.P.H. Hasselman and F.F. Lange, N.Y., Plenum Press (1974).

[16] Graham, L.J. and Alers, G.A., "Microstructural Aspects of Acoustic Emission Generation in Ceramics", Fracture Mechanics of Ceramics vol. 1, edited by R.C. Bradt, D.P.H. Hasselman and F.F. Lange, N.Y., 1974.

[17] Gillis,P.P. and Hamstad, M.A., "Mat. Sciences and Engineering, vol. 14, 1974, pp. 103-108.

[18] Evans, A.G. and Graham, L.G., "A Model for Crack Propagation in Polycrystalline Ceramics", Acta Metallurgica, vol. 23, 1975, pp. 1303-1311.

[19] Tandon, K.N. and Tangri, K., "Acoustic Emission During the Deformation of Polycrystalline Silicon-Iron", Materials Science and Engineering, 20, 1975, pp. 52-53.

[20] Copely, S.M. and Pask, J.A., "Deformation of Polycrystalline Ceramics", Mat. Science and Research vol. 3, chapter 13, edited by W.W. Kriegel and H. Palmour, N.Y. 1966, p. 215.

[21] Zener, C., "Fracturing of Metals", A.S.M., (1948), Cleveland, p. 3-31.

[22] Petch, N.J., "Fracture", edited by H. Liebowitz, vol. 1, London 1968, pp. 351-392.

[23] Averback, B.L., "Some Physical Aspects of Fracture", "Fracture", Chapter 7, edited by H. Liebowitz, vol. 1, 1963, p. 441.

[24] Ibid ....., pp. 442-471.

[25] Kear, B.H., Taylor, A. and Pratt, P.L., "Some Dislocation Interactions in Simple Ionic Crystals", Phil. Mat. (1959), vol. 4, p. 667.

[26] Conrad, H. and Stofel, E., "Modern Ceramics", Chapter 6, p. 173, edited by J.E. Hove and W.C. Riley, N.Y., John Wiley (1965).

[27] Marsh, D.M., "Fracture of Solids", proceedings of International Conference sponsored by The Institute of Metals, A.M. Institute of Minn., Met. and petroleum Engineers, edited by D.C. Drucker and J.J. Bilman (1962), p. 119.

[28] Low, J.R., "Fracture of Solids", proceedings of International Conference sponsored by The Institute of Metals, A.M. Institute of Minn., Met. and Petroleum Engineers, edited by D.C. Drucker, J.J. Gilman (1962), p. 201.

[29] Marsh, D.M., "Fracture of Solids", proceedings of International Conference sponsored by The Institute of Metals, A.M. Institute of Minn. Met. and Petroleum Engineers, edited by D.C. Drucker and J.J. Gilman (1962).

[30] Evans, A.G. and Davidge, R.W., "The Strength and Fracture of Fully Dense Polycrystalline MgO", Phil. Mag., 20, 1969, p. 373.

[31] Petch, N.J., "Cleavage Strength of Polycrystals", J. Iron and Steel Inst., vol. 14, pp. 25-28 (1953).

[32] Carniglia, S.C., "Re-examination of Experimental Strength vs. Grain Size Data for Ceramics", Am. Cer. Society vol. 55, No. 5, 1972, pp. 243-249.

[33] Sinha, M.N., Lloyd, D.J. and Tangri, K., "Microyield and Fracture in Polycrystalline MgO", J. of Mat. Science, 8, 1973, pp. 116-122.

[34] Fotedar, H.L., Srinivasan, M., Wilson, D.A. and Stoebe, T.G., "Specimen Geometry Effects and Deformation Characteristics in Ionic Crystals", Mat. Science and Engineering, 7 (1971), pp. 272-277.

[35] Ibrahim, N.A. and Tangri, K., "Influence of Irraditaion on Microyielding and Fracture of Polycrystalline MgO", Phil. Mag. in press.

[36] Evans, A.G., Wiederhorn, S.M., Linzer, M. and Fuller, E.R. Jr., "The Proof Testing of Porcelain Insulators and Application of Acoustic Emission", NBSIR 74-512, Inorganic Materials Division, Institute for Materials Research, National Bureau of Standards, U.S.A., p. 9.

[37] Frederick, J.R. and Felbeck, D.K., "Dislocation Motion as a Source of Acoustic Emission", Acoustic Emission STP 505, edited by R.G. Liptai, D.O. Harris and C.A. Tatro, ASTM (1972), pp. 129-139.

[38] Tetelman, A.S. and Chow, R., "Acoustic Emission Testing and Microcracking Processes", Acoustic Emission STP 505, edited by R.G. Liptai, D.O. Harris and C.A. Tatro, ASTM (1972), pp. 30-39.

APPENDIX I

Example of Grain Size Calculation

The term grain size is commonly used to denote the average grain diameter. The line intercept method was used to determine the average grain diameter. An important feature of this technique was: it averaged any orientation effect in the grain structure, since not all grains were cut through their greatest diameter.

The polished surface of a specimen was examined visually by an optical microscope. Four different micrographs were taken for different representative areas on the surface. More photographs were taken whenever any scatter in the grain size was observed. Each micrograph was studied separately as follows: five random traverse lines were drawn, then the number of grains intercepting each line was counted. This is done separately for each traverse line. The total length of the traverse lines was determined together with the total number of intercepting grains. The average grain diameter (D) was calculated using the relationship:

$$(D) = \frac{\text{Real length of the traverse lines}}{\text{Total number of intercepting grains}}$$

The following example illustrates this method:

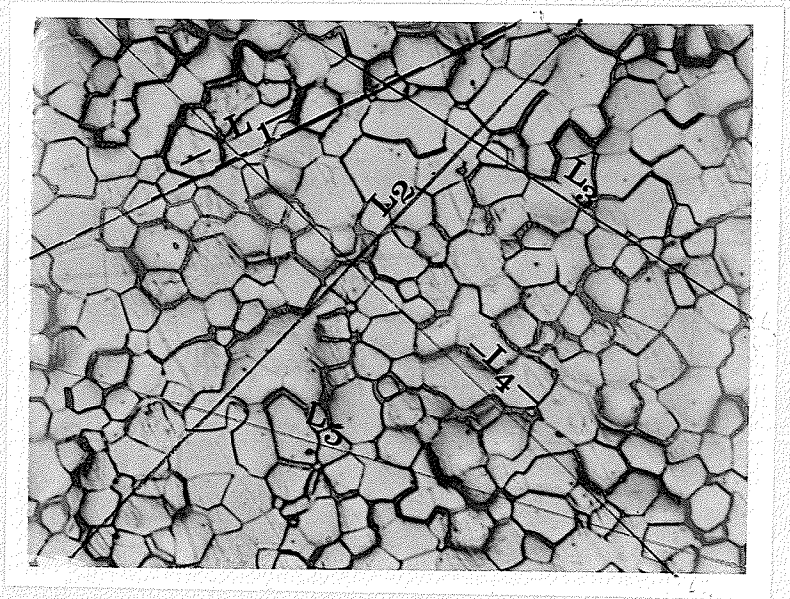

Length of the traverse line	Total number of grains
L_1 = 7.3 cm	15 grain
L_2 = 9.8 cm	21
L_3 = 7.4 cm	17
L_4 = 10.3 cm	23
L_5 = 9.5 cm	23

Total length of traverse lines = 44.3×10^6 microns

Total number of grains = 99

Magnification = 200

$$D = \frac{44.3}{99 \times 200} = 22.3 \times 10^{-6} \text{ cm} = 22.3 \text{ microns}$$

APPENDIX II

Operating Conditions of The Compression Jig

A special jig was designed for the uniaxial compression tests performed on polycrystalline MgO (Fig. 6). It has the following features: firstly, it can be used for high temperature testing up to 900 ^{o}C, and secondly, it has the capabilities of measuring strain using the LVDT technique and of collecting the acoustic emission signals by a transducer clipped at the bottom grip.

Several design considerations have restricted the selection of materials and dimensions. These are: a) the maximum operating temperature of the transducer which sets the allowable temperature limit at the transducer - grip interface, b) the thermal properties of the grips material, c) the mechanical properties; namely, the yield stress of the grip material since it should withstand stresses higher than the maximum fracture stress of the specimens.

To satisfy these requirements, several calculations were made to evaluate the stresses in the different parts of the jig to determine the dimensions and to study the heat transfer phenomenon together with the effect of cooling to select the grip materials. A compromise was made between the mechanical and thermal properties of the selected materials. Cooling coils were designed to ensure a temperature of 70 ^{o}C to be attained at the transducer - grip interface. The strength condition was satisfied by the selection of a high strength stainless steel with relatively low thermal conductivity.

Data:

Maximum temperature at the specimen:	900 ^{o}C
Maximum temperature at the transducer - grip interface:	70 ^{o}C

Internal diameter of the cooling coils: 3 mm

Amount of water in the cooling coils: 280 ml/second

Materials used for manufacturing the jig:

1. Grips: austenitic stainless steel, type 316
2. parts: austenitic stainless steel, type 302.